Bioorganic Chemistry 93 (2019) 103322

Contents lists available at ScienceDirect

Bioorganic Chemistry

journal homepage: www.elsevier.com/locate/bioorg

Design, synthesis and biological evaluation of novel copper-chelating acetylcholinesterase inhibitors with pyridine and *N*-benzylpiperidine fragments

Yeheng Zhou[a,d,1], Wei Sun[a,1], Jiale Peng[d], Hui Yan[a], Li Zhang[d], Xingyong Liu[d], Zhili Zuo[a,b,c,d,*]

[a] State Key Laboratory of Phytochemistry and Plant Resources in West China, Kunming Institute of Botany, Chinese Academy of Sciences, Kunming 650201, PR China
[b] Yunnan Key Laboratory of Natural Medicinal Chemistry, Kunming 650201, PR China
[c] University of Chinese Academy of Sciences, Beijing 100049, PR China
[d] School of Chemical Engineering, Sichuan University of Science & Engineering, Zigong 643000, PR China

ARTICLE INFO

Keywords:
Acetylcholinesterase
Drug design
N-acylhydrazone
Dementia
Copper-chelating
N-Benzylpiperidine

ABSTRACT

Cholinergic depletion is the direct cause of disability and dementia among AD patients. AChE is a classical and key target of cholinergic disorders. Some new inhibitors of AChE combining pyridine, acylhydrazone and *N*-benzylpiperidine fragments were developed in this work. The hit structure was optimized to yield the compound **21** with an IC_{50} value of 6.62 nM against AChE, while almost no inhibitory effect against BChE. ADMET predictions and PAMPA permeability evaluation showed good drug-like property. The higher activity with an intermediate alkyl chain substitution indicates a new binding mode of inhibitor with AChE. This finding provides new insights into the binding mechanism and is helpful for discovery of novel high-activity AChE inhibitors.

1. Introduction

Alzheimer's disease (AD) is one of the most popular cause of dementia, accounting for 60–80% of the total number of people with dementia worldwide [1]. Statistics show that there would be one more dementia patients every 3 s in the world [2]. The high cost of medicine and healthcare is a huge burden on the world economy and society. However, due to the complex pathogenesis of AD, there is no effective drug to date to cure the disease. Drugs that retard or stop the progress of AD only are available, such as AChE inhibitors donepezil and pyridostigmine. Therefore, the development of new AD treatment drugs is still a hot research area.

The most important anatomic pathological feature of AD is the overexpression of β-amyloid (Aβ) aggregated senile plaques and neurofibrillary tangles formed by misfolding of Tau protein after hyperphosphorylation [3]. Along with these two organic brain damages, an important neurotransmitter called acetylcholine (ACh) in the brain cells of AD patients is less than normal[4]. Because ACh plays an important role in many human neural activities, such as cognition, memory, dominating muscle movement, etc., the brain cholinergic system disorder in AD patients is the direct cause of disability and dementia. The cholinergic hypothesis is a classic hypothesis in the field of AD treatment. The most direct pathological factor is the loss of the neurotransmitter ACh caused by abnormal brain cholinergic system [3]. AChE is thus a very important target.

In addition, the metal ion hypothesis suggests that the steady-state dysregulation of metal ions is closely related to AD pathology [5–7]. In particular, steady-state dysregulation of redox-active Cu (I/II) and Fe (II/III) leads to excess reactive oxygen species (ROS) in the Fenton-like reaction, which in turn leads to oxidative stress in brain [8,9]. Among the many metal ions involved in the senile plaques (SPs), many studies have focused on Cu^{2+}, one of the major cationic elements in the formation of SPs [10,11]. Therefore, removal of Cu^{2+} may be helpful in the treatment of AD.

The *N*-acylhydrazone (NAH) is a kind of chemical structure which can chelate metal ions, and has both hydrogen bond acceptor and hydrogen bond donor. Until 2010, the therapeutic potential of the subfamily has been concerned by drug developers [12]. In particular, it is widely applied in drugs for the treatment of chronic pain, inflammatory diseases and cancer (Fig. 1), [13]. Nitrofurantoin is used as an oral antibacterial agent for the treatment of genitourinary tract infections [14]; carbazochrome has been used as a hemostatic agent for capillary and parenchymal hemorrhage [15]; azumolene sodium salt has good water solubility and can be used to treat malignant hyperthermia [16];

* Corresponding authors.
E-mail addresses: sunwei@mail.kib.ac.cn (W. Sun), liuxy@suse.edu.cn (X. Liu), zuozhili@mail.kib.ac.cn (Z. Zuo).
[1] Contribute equally to this work.

https://doi.org/10.1016/j.bioorg.2019.103322
Received 23 July 2019; Received in revised form 19 September 2019; Accepted 26 September 2019
Available online 26 September 2019

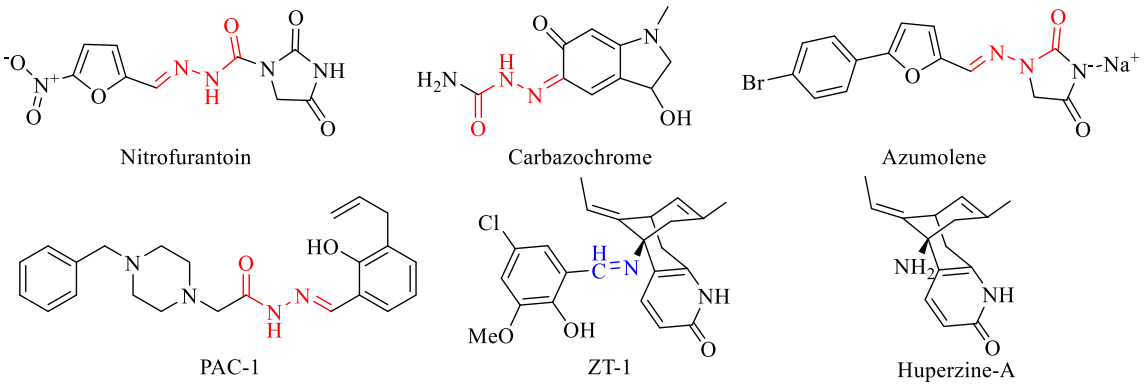

Fig. 1. Clinical and listed drugs containing hydrazide or imine groups.

PAC-1 has been used as a caspase activator and has entered the first phase of clinical use for anti-cancer [17]. ZT-1, which contains an imine structure, has been introduced into the clinical phase for the treatment of AD as a derivative of huperzine-A [18,19]. And it has better selectivity to other marketed medicines for AChE [20]. Its selectivity may be related to the imine group.

The selectivity of AChE inhibitor over BChE is an important issue in the drug discovery. Non-selective drug tacrine was withdrawn from the market because of hepatotoxicity [21]. Pyridostigmine, as an AChE inhibitor with poor selectivity, was found to cause adverse effects associated with vegetative nerve system [22]. Binding pocket analysis of AChE and BChE was shown in Fig. 2**(A)** and **(B)** respectively. The middle part of the AChE active cavity is a narrow channel (PDB code: 4EY7) [23], and the BChE receptor cavity is a tripartite star-shaped pocket (PDB code: 6QAA) [24]. Therefore, the molecular flexibility may be the main cause for its selectivity. In addition to the highly conserved catalytic triad [25], same amino acids are still present in both enzymes, and several identical amino acids at key sites are shown with green in Fig. 2.

Further analysis of the binding pocket of AChE complexed with donepezil revealed that there is possible a small space available in the tunnel part, especially around Asp-74. The distance between the methylene group (between the piperidine ring and indanone) of donepezil to the Asp-74 side chain carboxyl group was 5.8 Å. So, it is possible to introduce a small substitute at this position to improve the activity. After a try, this clue brought us a big surprise and implied a new binding mechanism.

Donepezil is the most classic AChE inhibitor in the current clinical treatment of AD. At present, a large number of studies have tried to design new inhibitors using donepezil as a template [26]. Pyridine alkaloids have good biological activity and are widely used in medicines, such as tipranavir and nexavar (shown in Fig. 3) [27,28]. Currently the mainstream academia has been trying hard to discover new AChE inhibitors with multiple functions, such as antioxidation [29], inhibition of Aβ aggregation [29–31], inhibition of hyaluronidase [31] and inhibition of monoamine oxidases (MAOs) [32]. Some examples with their IC_{50} value against electric eel acetyl cholinesterase (eeAChE) are listed in Fig. 4. In this study, some new structures combined *N*-benzylpiperidine moiety, a hydrazide group, and a pyridine ring have been developed. The activity and selectivity of the compound **21** performed better than the other function of compound **21** was the ability to chelate metal Cu^{2+}.

2. Results and discussion

The three dominant fragments were assembled to give template compound **1** (Fig. 5). The NAH linker provides both hydrogen bond acceptor (the imine) and hydrogen bond donor (the amide) to interact with AChE. We sought to optimize the structure based on the template of compound **1** by investigation of various type of A ring, B ring and the linker.

2.1. Chemistry

The structure–activity relationship of A ring was first explored. Commercially available benzoic acid, nicotinic acid, isonicotinic acid, and 2-picolinic acid were esterified to give methyl ester **1a-4a**, which were then reacted with hydrazine hydrate to give formylhydrazine intermediate **1b-4b**. The four formylhydrazides were condensed with commercially available benzyl-4-piperidone to give the corresponding acylhydrazones **1–4**. Microwave irradiation was used to increase the reaction rate and yield (see Scheme 1).

The length and flexibility of the linker in the middle were studied together with the position of nitrogen atom on the benzyl piperidine as shown in Scheme 2. The intermediates **5b** and **6b** were obtained by the Borch reduction reaction and the Dess-Martin oxidation reaction to change the position of the nitrogen atom on the *N*-benzyl-4-piperidone, and to change the length of the linker between the piperidine ring and the benzene ring. **5b** and **6b** were condensed with 2-pyridinecarboxhydrazide to obtain the corresponding acylhydrazones **5** and **6**. Furthermore, the intermediate **8a** was obtained by the Witting reaction according to the method described in the literature [33]. The double bond of intermediate **8a** was hydrogenated with Pd/C to give intermediate **9a**. **9a** was heated to reflux in THF with lithium aluminum hydride to yield the intermediate **9b**. The Dess-Martin oxidation reaction condition was modified to oxidize the intermediate **9b** to give the

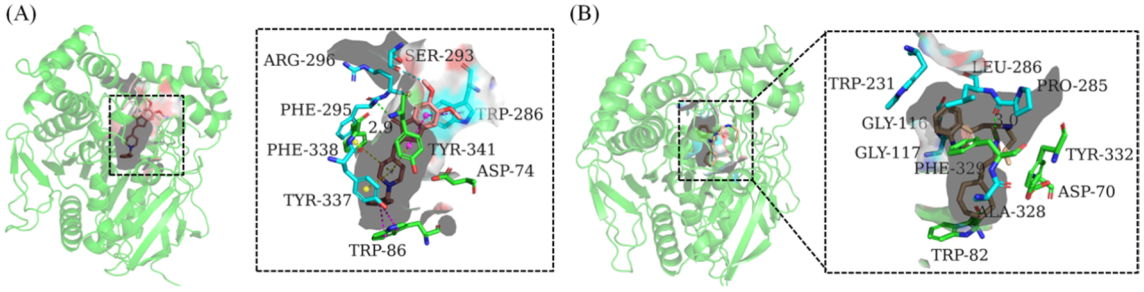

Fig. 2. Binding pocket analysis of AChE (A) and BChE (B).

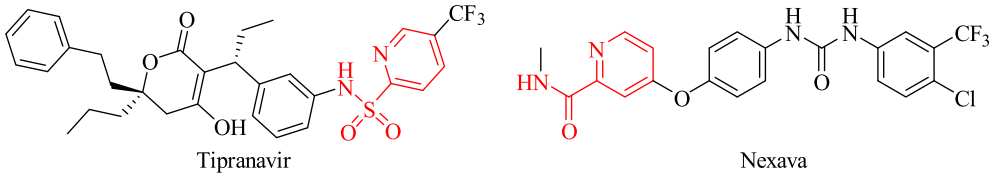

Fig. 3. The listed drug of Pyridine amide derivative.

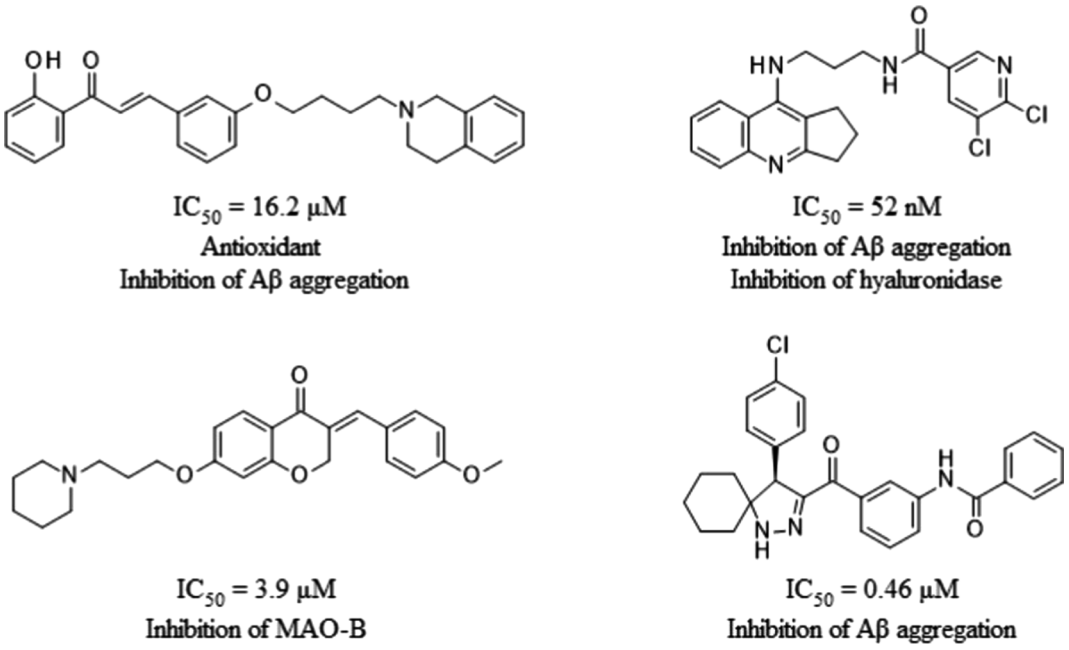

Fig. 4. Examples of multifunctional inhibitors and the IC_{50} values against eeAChE.

intermediate **9c**. Similar reaction route gave the intermediate **8c**. **8c** and **9c** were condensed with 2-pyridinecarboxhydrazide to obtain the corresponding acylhydrazones **8** and **9**. Commercially available *N*-benzylpiperidine-4-carboxaldehyde was directly condensed with 2-pyridinecarboxhydrazide to obtain the acylhydrazone **7**.

The modification of B ring was shown in Scheme 3. The electron-withdrawing and electron-pushing groups were introduced to investigate the effect of electrical properties on activity. Substituted aromatic aldehyde and 4-piperidinemethanol were subjected to a Borch reduction to give intermediate **10a-18a**. **10a-18a** was oxidized by the Dess-Martin reagent to give intermediates **10b-18b**. **10b-18b** were directly condensed with 2-pyridinecarboxhydrazide to obtain the corresponding acylhydrazones **10–18**. The *E*-conformation was determined by 2D-NMR (COSY and ROESY) with compound **10** as the example.

The introduction of the alkyl chain on the intermediate linker part was described in Scheme 4. The substituent was introduced to the amide of NAH according to the method described in the literature [34]. The methyl group was introduced by methyl iodide after the primary amine of the hydrazide was protected by phthalic anhydride. Deprotection gave the key intermediate **20c**. **20c** was condensed with 2-pyridinecarboxhydrazide to obtain acylhydrazone **20**. The alkyl chain was introduced to the aldehyde by the Grignard reaction to yield a secondary alcohol intermediate, which was then oxidized to **19b**, **21b-24b**. **19b** and **21b-24b** were condensed with 2-pyridinecarboxhydrazide to obtain the corresponding acylhydrazones **19, 21–24**. Trace of *Z*-conformation was introduced when compounds **19**, **21–24** were synthesized. The ratio of *E/Z* conformation was analyzed by the amide hydrogen with the aid of 2D-NMR (ROESY) (Supporting information). The percentage of *E*-conformation of all these compounds was the majority over 91.9%.

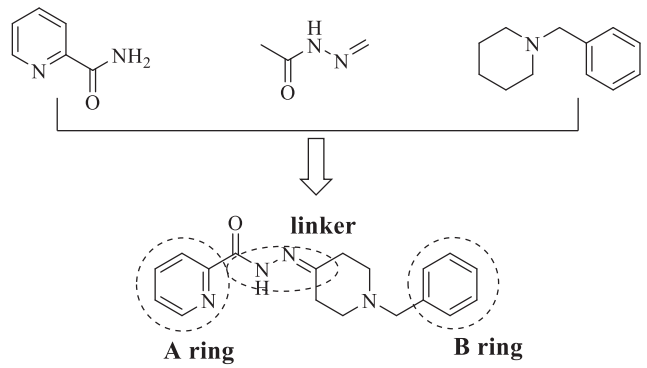

Fig. 5. Core skeleton design and optimization scheme.

2.2. Biological assays

2.2.1. In vitro inhibitory activities against AChE and BChE

The 24 compounds were evaluated against eeAChE and horse serum butyryl cholinesterase (eqBChE) using the method of Ellman et al.[35]. Donepezil and tacrine were used as the reference drugs.

Initially we looked into the effect of various A ring on compounds **1–4**. Only 2-picolinic acid derived compound **1** showed modest activity with an IC_{50} value of 135.0 μM, while the other aromatic acids derived compounds **2–4** gave poor inhibition with 50 μM concentration (Table 1). So, the optimization with 2-substituted pyridine as the fixed A ring was further carried out.

The length of the structure and activity of the AChE inhibitors were closely related [36,37]. We then investigated the spacer between the 2-substituted pyridine ring and the B ring. Shifting of the nitrogen atom from the piperidine to the exocyclic position (compound **5**) or insertion extra carbon between the piperidine ring and benzyl group (compound

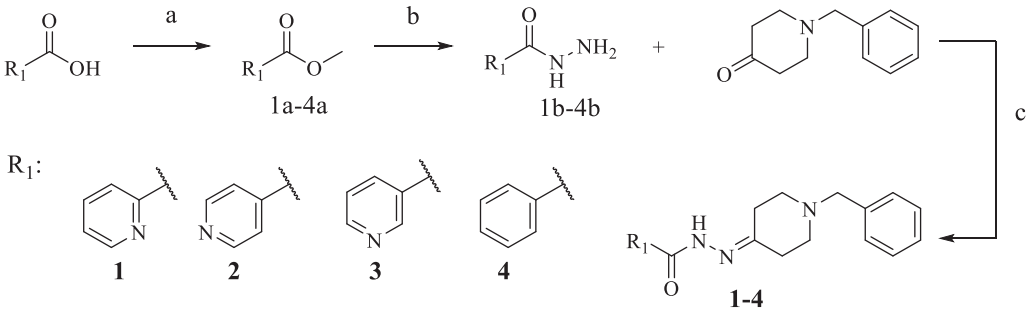

Scheme 1. The study of A ring in the structure. Reagents and conditions: (a) con. H_2SO_4 (2.5 V%), MeOH, Microwave, 30 min, Yield 87% (b) $N_2H_4{\cdot}H_2O$ (6 eq), 95 °C, Microwave, 30 min, Yield 95%. (c) aldehyde or ketone (1.05 eq), MeOH, 100 °C, microwave, 30 min, 80%

6) eliminated the inhibition, which indicated *N*-benzylpiperidine moiety from donepezil as the pharmacophore binding to the catalytic active site of AChE [38]. Elongation the NAH spacer by one carbon (compound **7**) dramatically improved the potency and gave 145-fold increase in the IC_{50} value (0.93 μM) compared to compound **1**. However, further elongation with two carbon atom length (compounds **8** and **9**) slightly reversed the inhibition increase tendency.

Selectivity between enzyme subtypes is an important issue in drug discovery. Compounds with improved selectivity between AChE and BChE may achieve better safety index[39,40]. So, the inhibition of BChE with compounds **7**, **8**, **9** and Donepezil was investigated in this work (Fig. 6). Dose-dependent effect was observed in all compounds with the concentration 200 μM, 100 μM, 50 μM and 25 μM. Compound **7** showing the weakest inhibition and Donepezil showing the strongest inhibition to BChE. Compound **7** was chosen as the template for further modification.

Synthesized compounds **7**, **8** and **9** inhibited BChE activity in a dose-dependent manner as donepezil did. The data represented the average of at least three different determinations with the indication of the standard error. The significance of the data was evaluated by *p* value (< 0.005).

Substitution on the benzene ring of the *N*-benzylpiperidine moiety had shown influence on the inhibition activity [41]. In this work, ortho-halogen substitution slightly promoted the potency with the chlorine-substituted compound **10** as the best example (IC_{50} = 0.55 μM) (Table 2). Electron-donating groups, such as methyl group (compound **17**) and methoxyl group (compound **14**), decreased the inhibition. 2,6-di-Cl substitution of the benzene ring (compound **18**), decreased the inhibition as well, which might be explained by the spatial limitation at the binding site.

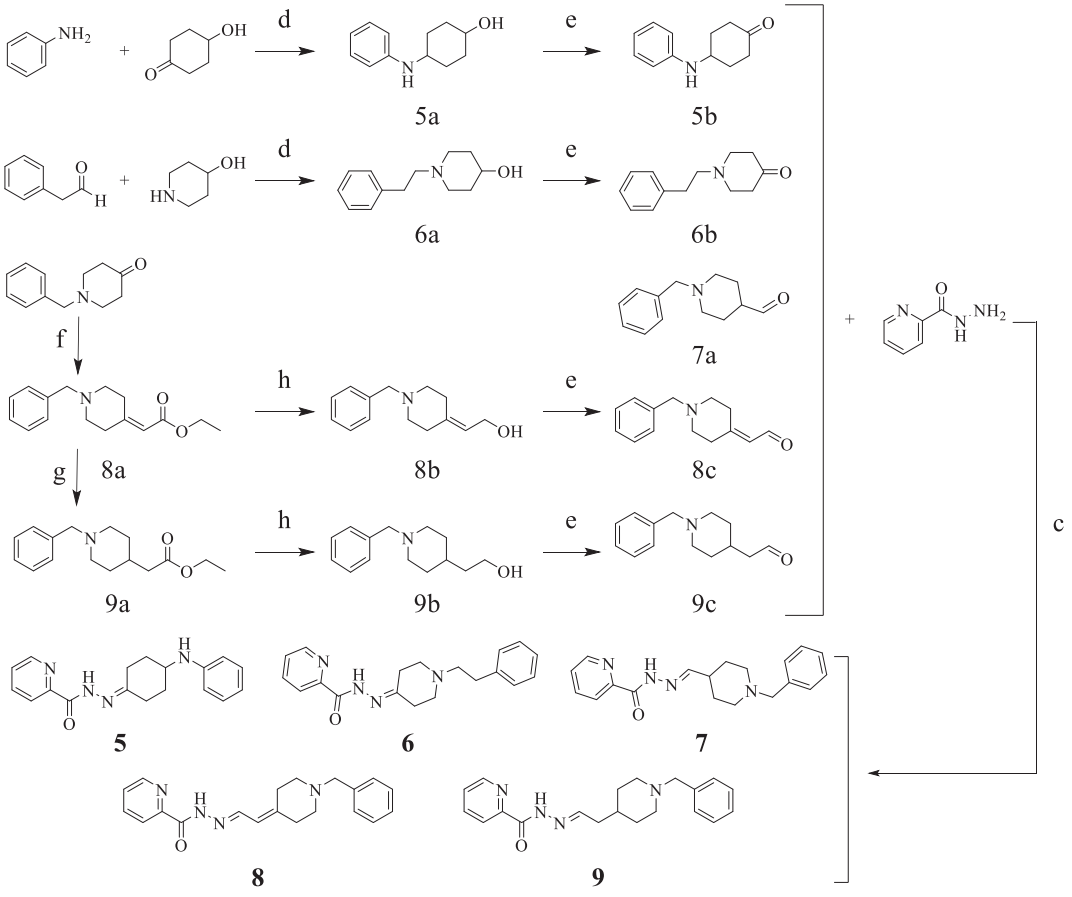

Scheme 2. Modification of the linker, and the position of nitrogen atom on the benzyl piperidine. Reagents and conditions: (d) $Na(A_cO)_3BH$ (1.6 eq), A_cOH (0.9 eq), DCM, rt, Overnight, yield 90%; (e) Dess-Matin reagent (2 eq), DCM, rt, 2 h; (f) $(EtO)_2POCH_2CO_2Et$ (1 eq), *n*-BuLi (1 eq), −70 °C, THF; (g) Pd/C (10% on activated carbon) (5 wt%), H_2, MeOH; (h) $LiAlH_4$, THF, reflux, 3 h.

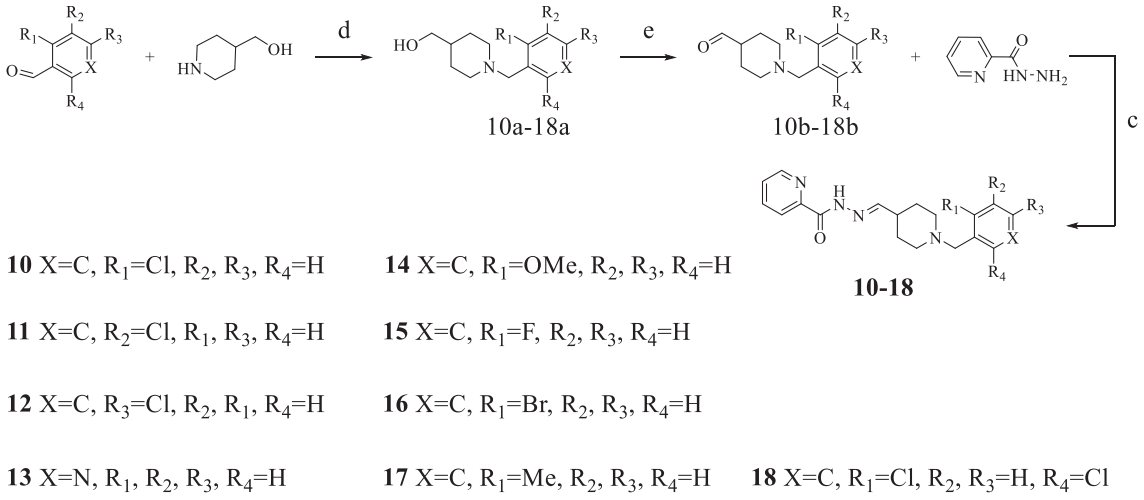

Scheme 3. The modification of B ring. Reagents and conditions: (d), (e) and (c) same as Scheme 2.

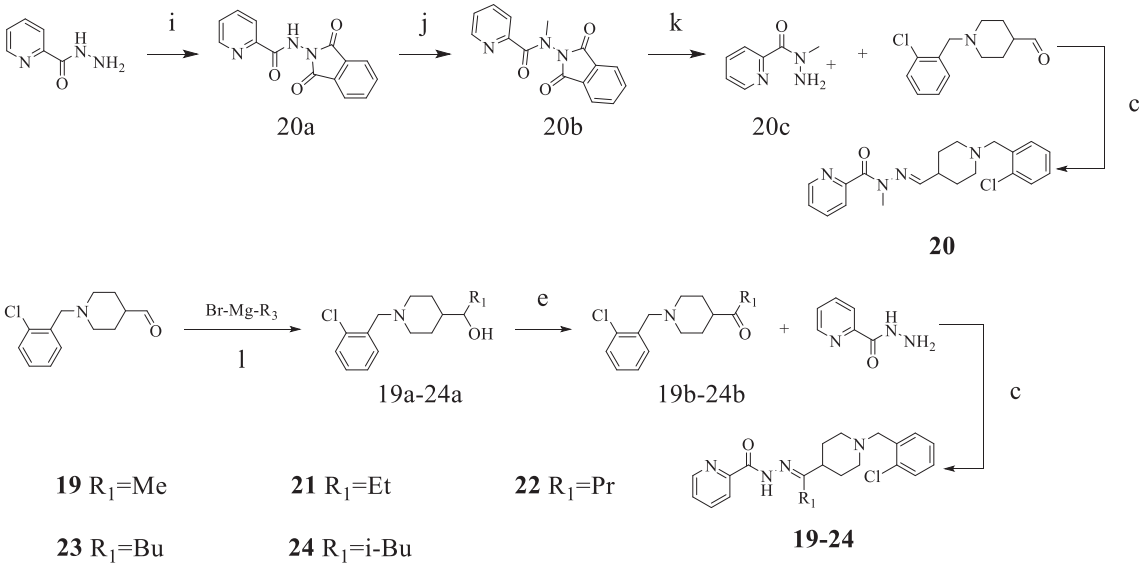

Scheme 4. The substitution of active hydrogen on the chain. Reagents and conditions: (i) phthalic anhydride, 130°C, 2 h, yield 93%; (j) ICH_3, acetone, 50°C, 18 h, yield 90%; (k) $N_2H_4{\cdot}H_2O$, MeOH, 50°C, yield 90%. (l) Grignard reagent (2 eq), THF, rt, overnight, yield 70%

Table 1
Inhibition of eeAChE by compounds **1–9**, tacrine and donepezil.

Compounds	inhibition rate (%)[a]	IC_{50}[b]
1	33.5 ± 0.7	135.02 ± 7.64 μM
2	2.0 ± 0.1	–
3	10.3 ± 0.3	–
4	2.5 ± 0.2	–
5	8.8 ± 0.1	–
6	13.6 ± 0.5	–
7	94.8 ± 0.0	0.93 ± 0.02 μM
8	90.8 ± 0.3	2.38 ± 0.08 μM
9	94.3 ± 0.1	1.98 ± 0.05 μM
Donepezil	–	20.55 ± 0.16 nM
Tacrine	–	59.73 ± 0.93 nM

[a] Inhibitory rate was measured with a final concentration of 50 μM of each compound against eeAChE, which was shown in Mean ± SD of triplicate wells.
[b] Concentration required for 50% inhibition of eeAChE, data were shown in Mean ± SD of triplicate independent experiments.

We sought to modify the NAH spacer on the template of compound **10** to explore possibility to further improve the potency. Methylation the amide nitrogen yielded compound **20**, which lost the inhibition activity (Table 2). However, introduction of a methyl group to the imine gave a 6-fold potency increase to yield compound **19** with the IC_{50} value of 92.46 nM. Further elongation of the methyl group to ethyl group and propyl group provided remarkable surprises to yield compound **21** (IC_{50} = 6.62 nM) and compound **22** (IC_{50} = 10.25 nM), respectively. A total of 83-fold improvement from compound **10** to compound **21** indicated that a ligand-induced-fit subpocket might form in the flexible tunnel of AChE through side-chain fluctuations. It was obvious that the volume of this ligand-induced-fit subpocket was limited because compounds **23** and **24** with larger alkyl groups showed a quick potency decrease. Meanwhile, the selectivity between AChE and BChE was maintained, which benefited from the structural rigidity of the NAH spacer. The selectivity index of the most potent compound **21** was over 3000-fold.

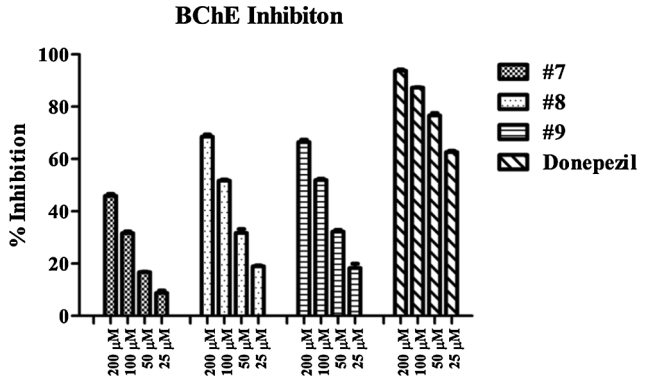

Fig. 6. Dose-dependent Inhibition of eqBChE by compounds **7–9**, and donepezil.

2.2.2. Kinetic characterization of AChE inhibition

The kinetic character describes the interaction patterns of ligands binding to enzymes. To explore the mechanism of AChE enzyme inhibition, the most potent compound **21** was subjected to an enzyme kinetic study together with donepezil. Lineweaver–Burk reciprocal plots were generated by plotting the reciprocal of the reaction rates versus the reciprocal of substrate concentrations using different concentrations of the test compounds (Fig. 7). The results suggested that compound **21** shared a similar non-competitive or mixed type of inhibition as donepezil.

2.2.3. Molecular docking study

In order to explore the binding mode of this class of compounds with AChE, the molecular docking study was carried out (Fig. 8**)**. Compounds **1** and **4** has a similar mode of action as donepezil. The pyridine ring forms a π-π interaction with Trp-286 and Tyr-341. The piperidine ring simultaneously forms a weak Pi-Alkyl interaction with Tyr-341, Phe-338, Tyr-337. The amide nitrogen forms a hydrogen bond with the phenolic hydroxyl group of Tyr-104, but failure to form a hydrogen bond with Phe-295 may be the main reason for its weaker activity than donepezil. Comparing the docking results of compounds **1** and **7**, it can be seen that the extension of compound **7** after prolonging one carbon leads to the closer distance between pyridine ring, carbonyl group and Phe-295, Arg-296. The position of carbonyl group allows the formation of a key hydrogen bond with Phe-295, and the nitrogen on the pyridine ring also forms hydrogen bond network with Phe-295, Arg-296. Thus, the activity is greatly increased by about 100 times. Comparing compounds **7** and **10**, it can be seen that after the introduction of the Cl atom at the 2-position of the benzyl group, Cl and Trp-86 form a weak halogen-Pi interaction, and thus the activity is slightly enhanced. Comparing compound **10** with compounds **19, 21,** and **22**, it can be seen that after the alkyl group is introduced, the alkyl group is inserted into the hydrophobic pocket formed by the three aromatic side chains of Tyr-104, Tyr-341 and Trp-286, and forms Pi-Alkyl interactions. So, the activity is greatly improved. Since the ethyl group is deeper than the methyl group, the activity is improved by 14 folds. But the propyl group is too bulky at this site. The activity test results is thus verified by the molecular docking study.

The binding conformation was further explored by taking the most active compound **21** as an example for BChE. Although the ligand in the crystal (PDB code: 6QAA) has a similar molecular length as compound **21**, compound **21** has almost no inhibition on BChE. In order to explore its selective mechanism, we conducted a molecular docking study of compound **21** with BChE protein. As shown in the Fig. 9, the docking result implies only a small part of compound **21** enters the binding pocket. The reason may due to the molecular rigidity of compound **21**, so that it cannot bend like HUN613 and forms a good binding conformation with BChE.

2.2.4. Prediction of ADME properties

Aqueous solubility, blood brain barrier (BBB) penetration, cytochrome P450 (CYP450) 2D6 inhibition, hepatotoxicity, and human intestinal absorption can be predicated using the ADMET Descriptors module in the Discovery Studio 4.0 (DS 4.0) software. A total of 6 key

Table 2
Inhibition of eeAChE and eqBChE by compounds **7**, **10–24**, tacrine and donepezil.

Compounds	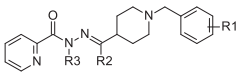			AChE inhibition rate (%) [a]	AChE inhibition IC_{50} [b]	BChE inhibition rate (%) [c]	Selectivity Index (SI) [d]
	R1	R2	*R3*				
7	H	H	H	94.8 ± 0.0	0.93 ± 0.02 μM	3.2 ± 1.1	> 21
10	*o*-Cl	H	H	86.2 ± 0.2	0.55 ± 0.04 μM	16.3 ± 0.8	> 36
11	*m*-Cl	H	H	49.4 ± 0.7	2.54 ± 0.06 μM	10.8 ± 0.4	> 7.9
12	*p*-Cl	H	H	2.8 ± 0.1	N/A	3.0 ± 1.6	N/A
13		H	H	13.5 ± 1.0	N/A	−7.0 ± 0.8	N/A
14	*o*-OMe	H	H	14.6 ± 0.2	N/A	21.0 ± 0.3	N/A
15	*o*-F	H	H	78.0 ± 0.3	0.58 ± 0.03 μM	5.7 ± 0.4	> 34
16	*o*-Br	H	H	73.9 ± 0.3	0.72 ± 0.02 μM	20.9 ± 1.0	> 27
17	*o*-Me	H	H	54.4 ± 0.6	1.90 ± 0.08 μM	43.6 ± 0.2	> 10
18	2,6-di-Cl	H	H	22.8 ± 0.9	N/A	10.9 ± 1.0	N/A
19	*o*-Cl	Me	H	27.6 ± 0.5	92.46 ± 2.97 nM	13.2 ± 0.5	> 216
20	*o*-Cl	H	Me	N/A	N/A	17.4 ± 0.5	N/A
21	*o*-Cl	Et	H	–	6.62 ± 0.38 nM	7.3 ± 0.7	> 3021
22	*o*-Cl	Pr	H	–	10.25 ± 0.45 nM	20.1 ± 0.6	> 1951
23	*o*-Cl	Bu	H	–	35.53 ± 1.40 nM	57.8 ± 0.1	N/A
24	*o*-Cl	*i*Bu	H	–	853.00 ± 8.43 nM	31.3 ± 0.4	> 23
Tacrine	–	–	–	–	59.73 ± 0.93 nM	22.99 ± 1.15 nM [e]	0.38
Donepezil	–	–	–	–	20.55 ± 0.16 nM	11.06 ± 0.55 μM [e]	538

[a] Inhibitory rate was measured with a final concentration of 5 μM of each compound against eeAChE, which was shown in Mean ± SD of triplicate wells.
[b] Concentration required for 50% inhibition of eeAChE, data were shown in Mean ± SD of triplicate independent experiments.
[c] Inhibitory rate was measured with a final concentration of 20 μM of each compound against eqBChE, and was shown in Mean ± SD of triplicate wells.
[d] Selectivity index (SI) is defined as eqBChE IC_{50}/eeAChE IC_{50}, and the eqBChE IC_{50} values of compounds **7**, **10–22** and **24** were derived to be over 20 μM from the inhibitory rates measured with the concentration of 20 μM.
[e] Concentration required for 50% inhibition of eqBChE, data were shown in Mean ± SD of triplicate independent experiments.

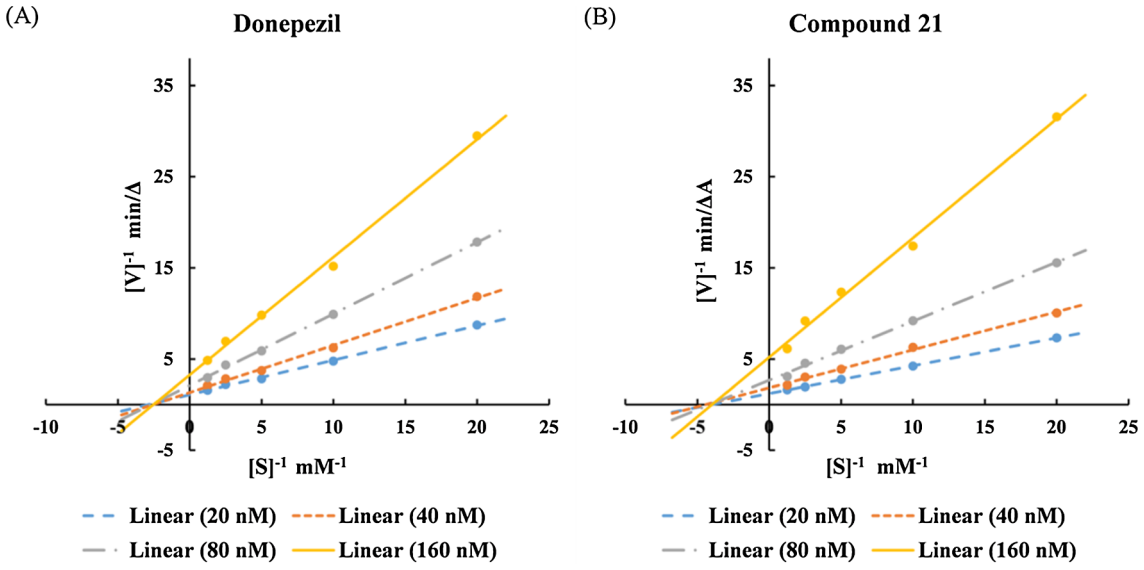

Fig. 7. Kinetic study of the mechanism of AChE inhibition. Lineweaver – Burk reciprocal plots of the AChE initial velocity at increasing substrate concentrations (0.05 mM, 0.1 mM, 0.2 mM, 0.4 mM, 0.8 mM) in the presence of donepezil and compound **21** (20 nM, 40 nM, 80 nM, 160 nM) are shown.

compounds **1, 7, 10, 19, 21** and **22** were selected and analyzed. The results as shown in Fig. 10, indicating that all compounds have good ADMET properties.

Some important parameters from the ADMET predictions were shown in Table 3. Compounds **1** and **7** showed good solubility, while compounds **10**, **19**, **21** and **22** showed low solubility. All six representative compounds have high blood-brain barrier permeability and no hepatotoxicity.

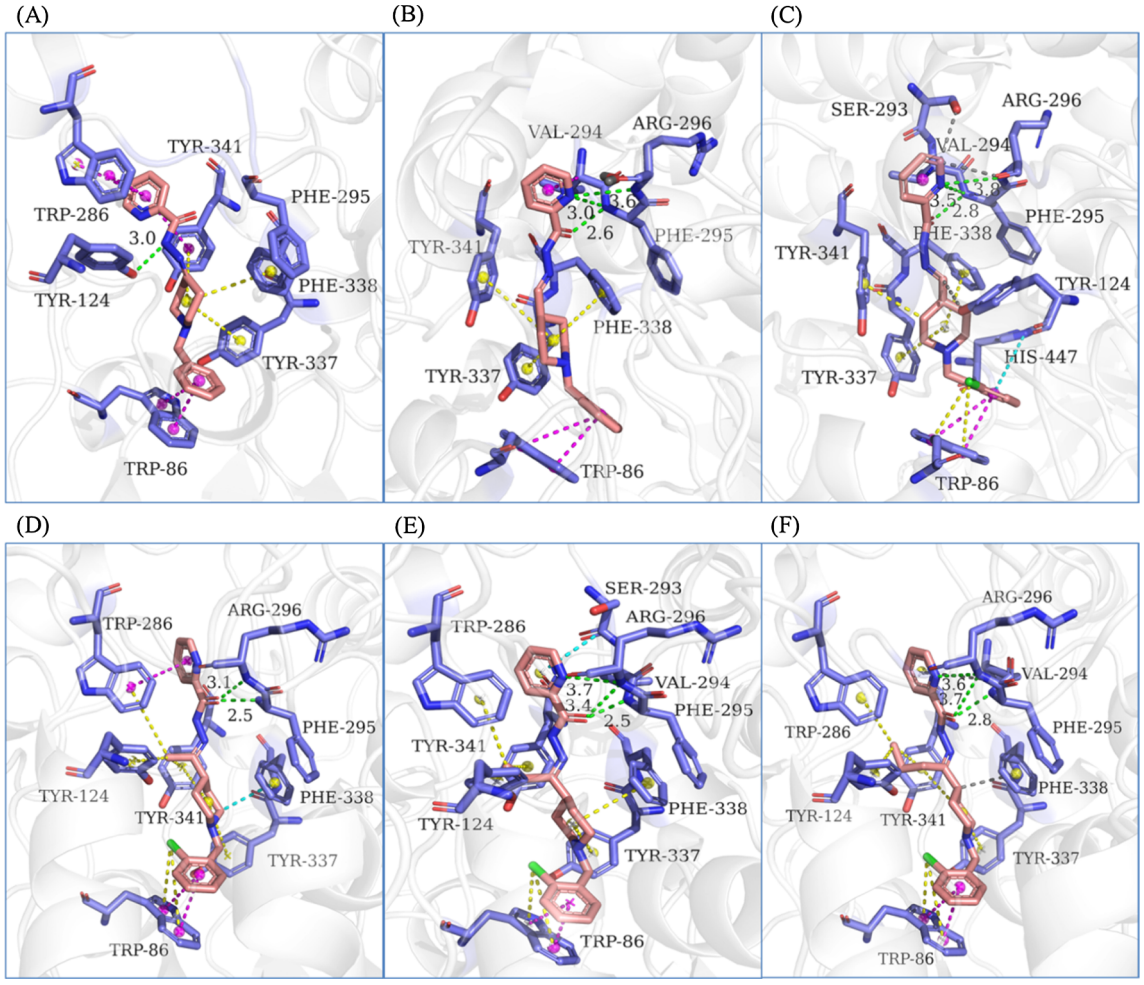

Fig. 8. The key interaction analysis of representative compounds. **A-F** illustrate the key interactions between compounds **1**, **7**, **10**, **19**, **21**, **22** and AChE, respectively.

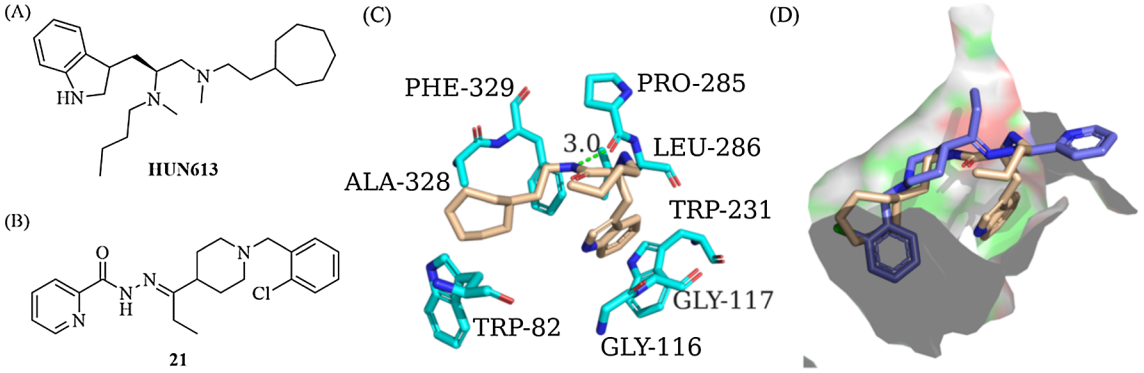

Fig. 9. Docking analysis of compound **21** and BChE.

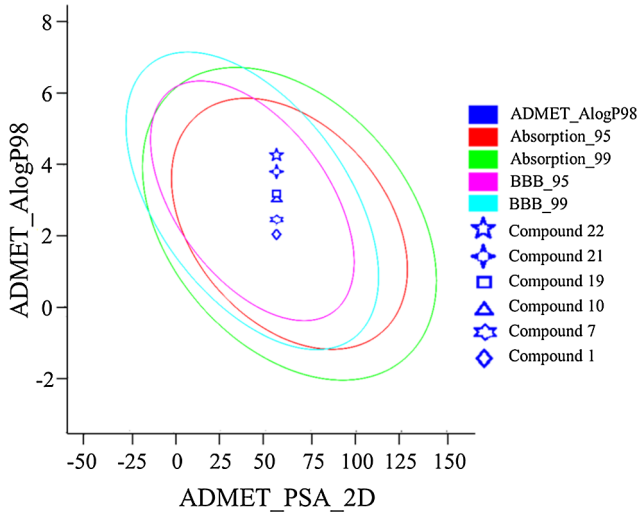

Fig. 10. The ADMET predictive analysis of the representative compounds.

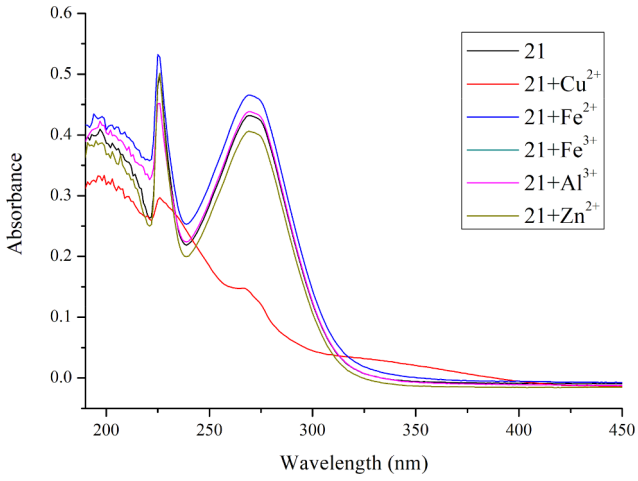

Fig. 11. The metal chelation ability test of compound **21**.

2.2.5. Capability to chelate copper ion

The chelation ability of compound **21** against metals such as Cu(II), Fe(II), Fe(III), Zn(II) and Al(III) was investigated by UV–visible spectroscopy (Fig. 11). The wavelength ranges from 190 nm to 600 nm. When $CuCl_2$ was added, the UV absorption peaks at both 226 nm and 267 nm wavelengths decreased significantly, indicating that **21** may form a complex with Cu^{2+}. However, there was no significant change after the addition of $FeCl_2$, $FeCl_3$, $AlCl_3$ and $ZnCl_2$.

2.2.6. PC12 cell toxicity evaluation

In vitro assessment of chemical induced toxicity to cells helps distinguish non-toxic hit compounds in the very early stage of drug discovery. PC12 cell line was originally isolated from a pheochromocytoma developed in the adrenal gland of an irradiated rat. Because PC12 cells treated with nerve growth factor (NGF) resemble sympathetic neurons, PC12 cells were utilized as a readily manipulable, easily grown experimental model for sympathetic neurons. Poorly differentiated PC12 cells have been used for cellular toxicity studies of neural

Table 3
PAMPA permeability and theoretical ADMET properties.

Compound	PAMPA[a]		BBB_Level[b]	Solubility Level[c]	EXT_Hepatotoxic #Prediction[d]
	Pe (10^{-6} cm/s)	R (%)			
1	3.23 ± 0.24	74.9 ± 0.8	2	3	FALSE
7	2.91 ± 0.49	7.3 ± 1.1	2	3	FALSE
10	6.09 ± 0.14	4.3 ± 2.2	2	2	FALSE
19	6.33 ± 0.32	8.0 ± 0.7	2	2	FALSE
21	6.72 ± 0.01	11.6 ± 0.6	1	2	FALSE
22	7.49 ± 0.14	9.2 ± 0.8	1	2	FALSE
Donepezil	6.54 ± 0.57	8.7 ± 1.1	–	–	–

[a] Effective permeability coefficients (Pe) and mass retention (R) were calculated as described. Results were given as Mean ± Standard Deviation (SD) of quintuplicate wells.

[b] Blood-brain barrier (BBB) penetration levels were predicted with Discovery Studio 4.0. There are four prediction levels: 0 (Very high/Brain-Blood ratio > 5:1), 1 (High/Brain-Blood ratio between 1:1 and 5:1), 2 (Medium/Brain-Blood ratio between 0.3:1 and 1:1) and 3 (Low/Brain-Blood ratio less than 0.3:1).

[c] Aqueous solubility levels were predicted with Discovery Studio 4.0. There are five prediction levels: 0 (Extremely low), 1 (Very low but possible), 2 (Low), 3 (Good), and 4 (Optimal).

[d] Hepatotoxic was predicted with Discovery Studio 4.0 and FALSE means that all properties and OPS components are within expected ranges.

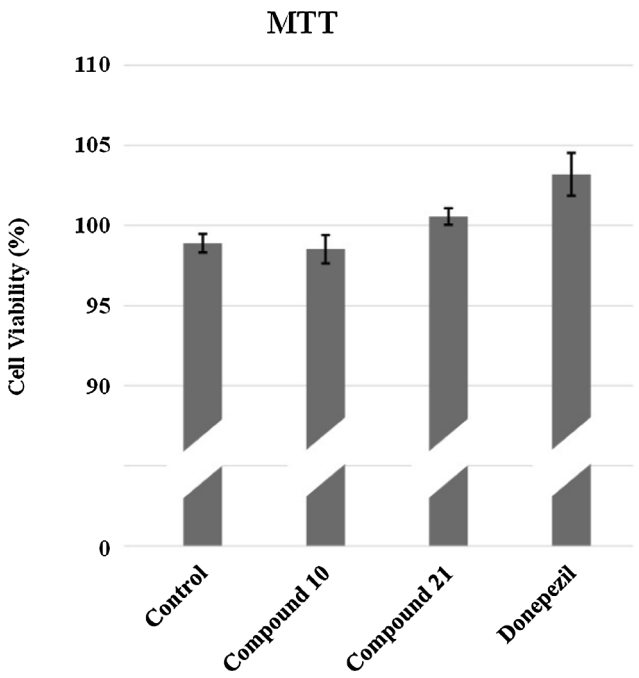

Fig. 12. Cytotoxicity data for compounds **10**, **21** and donepezil.

diseases [42]. We turned to utilize this cell line to evaluate the toxicity of compound **10** and compound **21** as well as the commercially available drug donepezil. As shown in Fig. 12, at a concentration of 20 μM, there was apparently no cytotoxicity. This result encourages further investigation of this series of potent AChE inhibitors.

2.2.7. Parallel artificial membrane permeability assay (PAMPA)

The ability to across biological membranes is a fundamental feature in the absorption and distribution of drugs. And it is the essential requirement for the central nervous system (CNS) drugs to penetrate the blood-brain barrier (BBB). PAMPA models were developed to evaluate the passive membrane permeability *in vitro*. Among the reported PAMPA models, the Corning Gentest™ Pre-coated PAMPA Plate System was widely utilized to assess compounds' passive transport ability through biological membranes, including numerous reports in CNS field [43–47]. The Corning Gentest™ Pre-coated PAMPA Plate System was used and the results were showed in Table 3 with donepezil as the reference compound. Compounds **10**, **19**, **21** and **22** demonstrated a significant increase of the passive membrane permeability in comparison with their parent compound **7** with normal mass retention ratio. A maximal 2.6-fold improvement was achieved. Since these synthesized compounds shared similar molecule volume and the same pharmacophore warhead with donepezil, the experimental Pe values all fell into the category (Pe $> 1.5 \times 10^{-6}$ cm/s), which represented a high permeability classification according to the literature [48].

3. Conclusion

In summary, the study involved the design, synthesis, and biological evaluation of a series of multifunctional agents against AD by fusing the *N*-benzylpiperidine moiety of donepezil and the pharmacophore of pyridine hydrazide. Most of the compounds have good inhibition of AChE and show very high selectivity over BChE. ADMET predictions show that this class of compounds has good drug-like properties. The most active compound **21** has an IC_{50} value of 6 nM and the capability to chelate cupric ion. All these results highlight that compound **21** is a promising lead compound for the development of anti-AD drugs. In particular, the introduction of an alkyl group to the NAH linker is considered to be a highlight of this study. The possible ligand-induced-fit sub-pocket in the tunnel part of AChE may provide new ideas for the development of novel high active AChE inhibitors.

4. Experimental section

4.1. Chemistry

All commonly used reagents and solvents are available from commercial suppliers and can be used directly. Thin layer chromatography (TLC) was performed using a GF-254 pre-formed high-performance silica gel plate to detect fluorescent spots at 254 nm UV light. Column chromatography silica gel was purchased from Qingdao Ocean Chemical Plant using 200–300 mesh. ^{1}H NMR and ^{13}C NMR spectra were measured separately at 25 °C using a two-dimensional spectrum Bruker AV III-400 or 600 spectrometer. The chemical shift is reported in ppm (d) using the remaining solvent line as an internal standard. Mass spectrometry and elemental analysis were performed using a Shimadzu Ultra Performance Liquid Chromatography -Ion Trap Time-of-Flight (UPLC-IT-TOF) chromatography mass spectrometer.

4.1.1. General procedure for the preparation of 1–24

All compounds were synthesized according to condition c (yield: 45–90%). This general procedure is described by using only Compound 1 as an example. Only the hydrogen, carbon and high-resolution mass spectra of all final products are listed in the article. See the supporting information for specific conditions and spectral data for intermediate synthesis. The reaction conditions were as follows: 0.5 ml of methanol, 22.23 mg (0.16 mmol) of intermediate 1b and 32.2 (0.17 mmol)mg of 4-benzylpiperidone were added to a 2 ml microwave tube and microwaved at 100 °C for 30 min. After the reaction was completed, the solvent was evaporated under reduced pressure. DCM/MeOH = 40:1 column chromatography gave 49.2 mg, yield 82.0%.

4.1.1.1. N'-(1-benzylpiperidin-4-ylidene)picolinohydrazide (1). ^{1}H NMR (400 MHz, $CDCl_3$) δ 2.54–2.74 (8H, m, J = 6.3 Hz), 3.58 (2H, s), 7.23–7.30 (1H, m), 7.30–7.40 (4H, m), 7.45 (1H, dd, J = 4.9, 6.5 Hz), 7.86 (1H, dt, J = 1.3, 7.7 Hz), 8.28 (1H, d, J = 7.8 Hz), 8.53 (1H, d, J = 4.4 Hz), 10.79 (1H, s). ^{13}C NMR (101 MHz, $CDCl_3$) δ 26.91, 34.77, 52.15, 53.44, 62.35, 122.82, 126.62, 127.31, 128.36, 129.05, 137.61, 137.90, 148.04, 149.45, 159.12, 159.99. HRMS (ESI): *m/z* 331.1528 $[M + Na]^+$; calcd for $C_{18}H_{20}N_4ONa$, 331.1529. Light yellow oily liquid, yield 82.0%.

4.1.1.2. N'-(1-benzylpiperidin-4-ylidene)isonicotinohydrazide (2). ^{1}H NMR (400 MHz, DMSO) δ 2.39–2.59 (8H, m) 3.56 (2H, s), 7.23–7.30 (1H, m), 7.34 (4H, d, J = 4.3 Hz), 7.73 (2H, d, J = 5.6 Hz), 8.72 (2H, d, J = 5.6 Hz), 10.97 (1H, s). ^{13}C NMR (101 MHz, DMSO) δ 28.76, 34.82, 52.45, 53.52, 61.65, 122.13, 127.47, 128.69, 129.24, 138.69, 141.50, 150.55, 162.26, 165.03. HRMS (ESI): *m/z* 331.1528 $[M + Na]^+$; calcd for $C_{18}H_{20}N_4ONa$, 331.1529. Light yellow solid, yield 45.0%.

4.1.1.3. N'-(1-benzylpiperidin-4-ylidene)nicotinohydrazide (3). ^{1}H NMR (400 MHz, DMSO) δ 2.27–2.59 (8H, m), 3.54 (2H, s), 7.22–7.29 (1H, m), 7.33 (4H, d, J = 4.3 Hz), 7.50 (1H, dd, J = 5.1, 7.2 Hz), 8.15 (1H, d, J = 7.7 Hz), 8.71 (1H, d, J = 3.9 Hz), 8.96 (1H, s), 10.89 (1H, s). ^{13}C NMR (101 MHz, DMSO) δ 28.66, 34.83, 52.47, 53.57, 61.70, 123.87, 127.46, 128.68, 129.23, 130.18, 135.93, 138.73, 149.05, 152.32, 162.42, 163.93. HRMS (ESI): *m/z* 309.1712 $[M + H]^+$; calcd for $C_{18}H_{21}N_4O$, 309.1710. Light yellow solid, yield 60.0%.

4.1.1.4. N'-(1-benzylpiperidin-4-ylidene)benzohydrazide (4). ^{1}H NMR (400 MHz, $CDCl_3$) δ 2.43–2.52 (2H, m), 2.54–2.71 (6H, m), 3.56 (2H, s), 7.23–7.30 (1H, m,), 7.33 (4H, d, J = 4.2 Hz), 7.42 (2H, t, J = 7.5 Hz), 7.50 (1H, t, J = 7.2 Hz), 7.78 (2H, d, J = 6.2 Hz), 8.90 (1H, s). ^{13}C NMR (101 MHz, $CDCl_3$) δ 27.11, 34.80, 52.08, 53.45, 62.37, 127.21, 127.28, 128.36, 128.73, 128.99, 131.85, 133.64,

138.06, 160.00, 164.25. HRMS (ESI): *m/z* 330.1576 $[M + Na]^+$; calcd for $C_{19}H_{21}N_4ONa$, 330.1577. Yellow-green solid, yield 90.0%.

*4.1.1.5. N'-(4-(phenylamino)cyclohexylidene)picolinohydrazide (**5**).* ^1H NMR (400 MHz, $CDCl_3$) δ 1.47–1.69 (2H, m), 2.20–2.37 (3H, m), 2.44–2.58 (1H, m), 2.77–2.94 (2H, m), 3.51–3.71 (2H, m), 6.64 (2H, d, J = 7.8 Hz), 6.72 (1H, t, J = 7.3 Hz), 7.20 (2H, t, J = 7.9 Hz), 7.44–7.50 (1H, m), 7.89 (1H, dt, J = 1.5, 7.7 Hz), 8.30 (1H, d, J = 7.8 Hz), 8.56 (1H, d, J = 4.3 Hz), 10.82 (1H, s). ^{13}C NMR (101 MHz, $CDCl_3$) δ 29.44, 38.98, 52.61, 55.52, 115.23 (1C, d, J = 22.2 Hz), 122.90 (1C, s), 123.87 (1C, d, J = 3.5 Hz), 124.67 (1C, d, J = 14.3 Hz), 126.68, 128.79 (1C, d, J = 8.3 Hz), 131.61 (1C, d, J = 4.5 Hz), 137.57, 148.00, 149.13, 155.52, 159.97, 161.40 (1C, d, J = 246.3 Hz). HRMS (ESI): *m/z* 309.1715 $[M + Na]^+$; calcd for $C_{18}H_{20}N_4ONa$, 309.1710. White solid, yield 74.6%.

*4.1.1.6. N'-(1-phenethylpiperidin-4-ylidene)picolinohydrazide (**6**).* ^1H NMR (400 MHz, $CDCl_3$) δ 2.59–2.66 (2H, m), 2.66–2.74 (6H, m), 2.74–2.79 (2H, m), 2.81–2.89 (2H, m), 7.18–7.26 (3H, m), 7.30 (2H, t, J = 7.5 Hz), 7.47 (1H, dd, J = 5.0, 6.9 Hz), 7.88 (1H, dt, J = 1.4, 7.7 Hz), 8.30 (1H, d, J = 7.8 Hz), 8.55 (1H, d, J = 4.5 Hz), 10.82 (1H, s). ^{13}C NMR (101 MHz, $CDCl_3$) δ 26.93, 33.88, 34.73, 52.43, 53.49, 59.74, 122.83, 126.18, 126.63, 128.45, 128.69, 137.62, 140.02, 148.04, 149.45, 158.93, 160.01. HRMS (ESI): *m/z* 345.1689 $[M + Na]^+$; calcd for $C_{19}H_{22}N_4ONa$, 345.1686. Yellow-green solid, yield 75%.

*4.1.1.7. (E)-N'-((1-benzylpiperidin-4-yl)methylene)picolinohydrazide (**7**).* ^1H NMR (400 MHz, $CDCl_3$) δ 1.58–1.73 (2H, m), 1.76–1.88 (2H, m), 1.99–2.12 (2H, m), 2.45–2.57 (1H, m,), 2.87–2.99 (2H, m), 3.51 (2H, s), 7.20–7.28 (1H, m), 7.32 (4H, d, J = 4.4 Hz), 7.42–7.50 (2H, m), 7.87 (1H, dt, J = 1.5, 7.7 Hz), 8.27 (1H, d, J = 7.8 Hz), 8.53 (1H, d, J = 4.4 Hz), 10.66 (1H, s). ^{13}C NMR (101 MHz, $CDCl_3$) δ 29.47, 39.16, 52.85, 63.39, 122.93, 126.69, 127.05, 128.23, 129.21, 137.59, 138.20, 148.00, 149.13, 155.64, 159.98. HRMS (ESI): *m/z* 345.1684 $[M + Na]^+$; calcd for $C_{19}H_{22}N_4ONa$, 345.1686. Gray-white solid, yield 80%.

*4.1.1.8. (E)-N'-(2-(1-benzylpiperidin-4-ylidene)ethylidene)picolinohydrazide (**8**).* ^1H NMR (400 MHz, $CDCl_3$) δ 2.36–2.43 (2H, m), 2.46–2.58 (6H, m), 3.53 (2H, s), 6.22 (1H, d, J = 9.8 Hz), 7.23–7.29 (1H, m), 7.30–7.40 (4H, m), 7.43–7.49 (1H, m), 7.87 (1H, dt, J = 1.5, 7.7 Hz), 8.19 (1H, d, J = 9.8 Hz), 8.28 (1H, d, J = 7.8 Hz), 8.54 (1H, d, J = 4.5 Hz), 10.78 (1H, s). ^{13}C NMR (101 MHz, $CDCl_3$) δ 29.28, 36.49, 53.98, 54.64, 62.61, 120.04, 122.91, 126.66, 127.20, 128.30, 129.12, 137.61, 146.58, 147.99, 149.15, 150.27, 159.91. HRMS (ESI): *m/z* 335.1868 $[M+H]^+$; calcd for $C_{20}H_{23}N_4O$, 335.1866. Brown oily liquid, yield 65%.

*4.1.1.9. (E)-N'-(2-(1-benzylpiperidin-4-yl)ethylidene)picolinohydrazide (**9**).* ^1H NMR (400 MHz, $CDCl_3$) δ 1.34–1.46 (2H, m), 1.56–1.66 (1H, m), 1.70 (2H, d, J = 13.2 Hz), 1.96 (2H, t, J = 11.1 Hz), 2.40 (2H, t, J = 6.3 Hz), 2.88 (2H, d, J = 11.4 Hz), 3.49 (2H, s), 7.21–7.26 (1H, m), 7.27–7.34 (4H, m), 7.43–7.49 (1H, m), 7.64 (1H, t, J = 5.9 Hz), 7.87 (1H, dt, J = 1.5, 7.7 Hz), 8.29 (1H, d, J = 7.8 Hz), 8.54 (1H, d, J = 4.4 Hz), 10.69 (1H, s). ^{13}C NMR (101 MHz, $CDCl_3$) δ 32.07, 34.51, 38.90, 53.58, 63.37, 122.94, 126.68, 126.98, 128.18, 129.22, 137.59, 138.29, 148.00, 149.13, 151.83, 159.91. HRMS (ESI): *m/z* 337.2024 $[M+H]^+$; calcd for $C_{19}H_{23}N_4O$, 337.2023. White solid, yield 70%.

*4.1.1.10. (E)-N'-((1-(2-chlorobenzyl)piperidin-4-yl)methylene) picolinohydrazide (**10**).* ^1H NMR (400 MHz, $CDCl_3$) δ 1.62–1.76 (2H, m), 1.83 (2H, d, J = 11.5 Hz), 2.16 (2H, t, J = 10.7 Hz), 2.47–2.59 (1H, m,), 2.94 (2H, d, J = 11.4 Hz), 3.61 (2H, s), 7.13–7.26 (2H, m), 7.31–7.35 (1H, m), 7.41–7.57 (3H, m), 7.87 (1H, dt, J = 1.5, 7.7 Hz), 8.28 (1H, d, J = 7.8 Hz), 8.53 (1H, d, J = 4.4 Hz), 10.66 (1H, s). ^{13}C NMR (101 MHz, $CDCl_3$) δ 29.50, 39.07, 52.93, 59.47, 122.92, 126.62, 126.68, 128.11, 129.40, 130.70, 134.27, 135.98, 137.58, 148.00, 149.14, 155.53, 159.97. HRMS (ESI): *m/z* 379.1302 $[M+Na]^+$; calcd for $C_{19}H_{21}N_4OClNa$, 379.1279. Gray-white solid, yield 80%.

*4.1.1.11. (E)-N'-((1-(3-chlorobenzyl)piperidin-4-yl)methylene) picolinohydrazide (**11**).* ^1H NMR (400 MHz, $CDCl_3$) δ 1.60–1.74 (2H, m), 1.85 (2H, d, J = 11.2 Hz), 2.02–2.13 (2H, m), 2.47–2.59 (1H, m,), 2.92 (2H, d, J = 11.5 Hz), 3.49 (2H, s), 7.17–7.30 (3H, m), 7.35 (1H, s), 7.48 (2H, t, J = 6.7 Hz), 7.89 (1H, dt, J = 1.5, 7.7 Hz), 8.30 (1H, d, J = 7.8 Hz), 8.56 (1H, d, J = 4.4 Hz), 10.69 (1H, s). ^{13}C NMR (101 MHz, $CDCl_3$) δ 29.41, 39.06, 52.84, 62.67, 122.91, 126.69, 127.18, 127.23, 129.02, 129.49, 134.15, 137.58, 140.53, 148.01, 149.12, 155.45, 159.99. HRMS (ESI): *m/z* 357.1478 $[M+H]^+$; calcd for $C_{19}H_{22}N_4OCl$, 357.1477. Yellow-brown solid, yield 60%.

*4.1.1.12. (E)-N'-((1-(4-chlorobenzyl)piperidin-4-yl)methylene) picolinohydrazide (**12**).* ^1H NMR (400 MHz, $CDCl_3$) δ 1.43–1.57 (2H, m), 1.69 (2H, d, J = 12.1 Hz), 1.90 (2H, t, J = 10.9 Hz), 2.31–2.43 (1H, m,), 2.75 (2H, d, J = 11.4 Hz), 3.32 (2H, s), 7.08–7.18 (4H, m), 7.33 (2H, t, J = 5.7 Hz), 7.71–7.78 (1H, m), 8.14 (1H, d, J = 7.8 Hz), 8.40 (1H, d, J = 4.3 Hz), 10.53 (1H, s). ^{13}C NMR (101 MHz, $CDCl_3$) δ 29.41, 39.07, 52.79, 62.51, 122.92, 126.70, 128.37, 130.43, 132.74, 136.77, 137.59, 148.01, 149.11, 155.45, 159.99. HRMS (ESI): *m/z* 357.1478 $[M+H]^+$; calcd for $C_{19}H_{22}N_4OCl$, 357.1477. Light yellowish brown solid, yield 65%.

*4.1.1.13. (E)-N'-((1-(pyridin-3-ylmethyl)piperidin-4-yl)methylene) picolinohydrazide (**13**).* ^1H NMR (400 MHz, $CDCl_3$) δ 1.56–1.70 (2H, m), 1.83 (2H, d, J = 11.7 Hz), 2.07 (2H, t, J = 10.7 Hz), 2.44–2.56 (1H, m), 2.89 (2H, d, J = 11.4 Hz), 3.50 (2H, s), 7.22–7.26 (1H, m), 7.41–7.50 (2H, m), 7.66 (1H, d, J = 7.7 Hz), 7.86 (1H, dt, J = 1.3, 7.7 Hz), 8.27 (1H, d, J = 7.8 Hz), 8.47–8.55 (3H, m), 10.67 (1H, s). ^{13}C NMR (101 MHz, $CDCl_3$) δ 29.45, 39.07, 52.86, 60.51, 122.93, 123.33, 126.70, 133.83, 136.71, 137.60, 148.00, 148.56, 149.10, 150.44, 155.39, 159.99. HRMS (ESI): *m/z* 346.1633 $[M+Na]^+$; calcd for $C_{18}H_{21}N_5ONa$, 346.1638. Gray-white solid, yield 75%.

*4.1.1.14. (E)-N'-((1-(2-methoxybenzyl)piperidin-4-yl)methylene) picolinohydrazide (**14**).* ^1H NMR (400 MHz, $CDCl_3$) δ 1.60–1.73 (2H, m), 1.81 (2H, d, J = 10.9 Hz), 2.11 (2H, t, J = 10.8 Hz), 2.44–2.56 (1H, m,), 2.97 (2H, d, J = 11.6 Hz), 3.57 (2H, s), 3.82 (3H, s), 6.87 (1H, d, J = 8.2 Hz), 6.93 (1H, t, J = 7.3 Hz), 7.18–7.25 (1H, m), 7.35 (1H, d, J = 7.4 Hz), 7.40–7.50 (2H, m), 7.87 (1H, dt, J = 1.4, 7.7 Hz), 8.28 (1H, d, J = 7.8 Hz), 8.53 (1H, d, J = 4.4 Hz), 10.65 (1H, s). ^{13}C NMR (101 MHz, $CDCl_3$) δ 29.49, 39.12, 52.81, 55.45, 56.28, 110.47, 120.32, 122.90, 126.15, 126.67, 128.07, 130.60, 137.57, 148.00, 149.15, 155.79, 157.82, 159.97. HRMS (ESI): *m/z* 353.1975 $[M+H]^+$; calcd for $C_{20}H_{25}N_4O_2$, 353.1972. Light yellowish brown solid, yield 77%.

*4.1.1.15. (E)-N'-((1-(2-fluorobenzyl)piperidin-4-yl)methylene) picolinohydrazide (**15**).* ^1H NMR (400 MHz, $CDCl_3$) δ 1.58–1.72 (2H, m), 1.83 (2H, d, J = 12.4 Hz), 2.11 (2H, t, J = 10.8 Hz), 2.43–2.56 (1H, m), 2.94 (2H, d, J = 11.5 Hz), 3.58 (2H, s), 7.03 (1H, t, J = 9.1 Hz), 7.10 (1H, t, J = 7.3 Hz), 7.20–7.26 (1H, m), 7.37 (1H, t, J = 6.9 Hz), 7.42–7.51 (2H, m), 7.87 (1H, dt, J = 1.4, 7.7 Hz), 8.28 (1H, d, J = 7.8 Hz), 8.53 (1H, d, J = 4.4 Hz), 10.65 (1H, s). HRMS (ESI): *m/z* 341.1770 $[M+H]^+$; calcd for $C_{19}H_{22}N_4OF$, 341.1772. White solid, yield 70%.

*4.1.1.16. (E)-N'-((1-(2-bromobenzyl)piperidin-4-yl)methylene) picolinohydrazide (**16**).* ^1H NMR (400 MHz, $CDCl_3$) δ 1.60–1.73 (2H, m), 1.84 (2H, d, J = 11.5 Hz), 2.18 (2H, t, J = 10.7 Hz), 2.47–2.59 (1H, m), 2.95 (2H, d, J = 11.5 Hz), 3.60 (2H, s), 7.07–7.15 (1H, m), 7.28 (1H, t, J = 7.3 Hz), 7.43–7.51 (3H, m), 7.53 (1H, d, J = 7.9 Hz), 7.88 (1H, dt, J = 1.5, 7.7 Hz), 8.29 (1H, d, J = 7.8 Hz), 8.55 (1H, d,

J = 4.4 Hz), 10.67 (1H, s). ^{13}C NMR (101 MHz, $CDCl_3$) δ 29.58, 39.13, 52.96, 62.08, 122.94, 124.61, 126.69, 127.21, 128.33, 130.65, 132.70, 137.60, 137.83, 148.01, 149.14, 155.60, 159.98. HRMS (ESI): *m/z* 401.0971 $[M+H]^+$; calcd for $C_{19}H_{22}N_4OBr$, 401.0971. Yellow-brown solid, yield 80%.

*4.1.1.17. (E)-N′-((1-(2-methylbenzyl)piperidin-4-yl)methylene) picolinohydrazide (**17**).* ^{1}H NMR (400 MHz, $CDCl_3$) δ 1.55–1.68 (2H, m), 1.81 (2H, d, J = 11.7 Hz), 2.07 (2H, t, J = 10.7 Hz), 2.46–2.57 (1H, m), 2.91 (2H, d, J = 11.5 Hz), 3.45 (2H, s), 7.11–7.19 (3H, m), 7.22–7.30 (1H, m), 7.42–7.51 (2H, m), 7.88 (1H, dt, J = 1.5, 7.7 Hz), 8.28 (1H, d, J = 7.8 Hz), 8.54 (1H, d, J = 4.4 Hz), 10.66 (1H, s). ^{13}C NMR (101 MHz, $CDCl_3$) δ 19.27, 29.66, 39.34, 53.01, 61.10, 122.94, 125.47, 126.68, 126.94, 129.75, 130.23, 136.69, 137.49, 137.60, 148.00, 149.14, 155.80, 159.98. HRMS (ESI): *m/z* 337.2025 $[M+H]^+$; calcd for $C_{20}H_{25}N_4O$, 337.2023. Yellow-brown solid, yield 70%.

*4.1.1.18. (E)-N′-((1-(2,6-dichlorobenzyl)piperidin-4-yl)methylene) picolinohydrazide (**18**).* ^{1}H NMR (400 MHz, $CDCl_3$) δ 1.52–1.67 (2H, m), 1.79 (2H, d, J = 11.9 Hz), 2.28 (2H, t, J = 11.0 Hz), 2.46–2.58 (1H, m), 2.96 (2H, d, J = 11.1 Hz), 3.74 (2H, s), 7.13 (1H, t, J = 8.0 Hz), 7.29 (2H, t, J = 9.1 Hz), 7.40–7.50 (2H, m), 7.87 (1H, dt, J = 1.4, 7.7 Hz), 8.28 (1H, d, J = 7.8 Hz), 8.54 (1H, d, J = 4.4 Hz), 10.64 (1H, s). ^{13}C NMR (101 MHz, $CDCl_3$) δ 29.54, 39.11, 52.79, 56.80, 122.92, 126.67, 128.34, 128.74, 134.62, 136.99, 137.58, 147.99, 149.14, 155.73, 159.96. HRMS (ESI): *m/z* 391.1087 $[M+H]^+$; calcd for $C_{19}H_{21}N_4OCl_2$, 391.1087. White solid, yield 85%.

*4.1.1.19. (E)-N′-(1-(1-(2-chlorobenzyl)piperidin-4-yl)ethylidene) picolinohydrazide (**19**).* ^{1}H NMR (400 MHz, $CDCl_3$) δ 1.72–1.81 (4H, m), 2.00 (3H, s), 2.08–2.20 (2H, m), 2.49–2.62 (1H, m), 2.98 (2H, d, J = 11.2 Hz), 3.60 (2H, s), 7.13–7.20 (1H, m), 7.23 (1H, t, J = 7.4 Hz), 7.33 (1H, d, J = 7.8 Hz), 7.42–7.53 (2H, m), 7.82–7.91 (1H, m), 8.28 (1H, d, J = 7.8 Hz), 8.54 (1H, d, J = 4.6 Hz), 10.71 (1H, s). ^{13}C NMR (101 MHz, $CDCl_3$) δ 12.72, 29.30, 45.42, 53.47, 59.50, 122.82, 126.56, 127.96, 129.36, 130.53, 134.19, 136.33, 137.56, 148.04, 149.61, 159.87, 161.15. HRMS (ESI): *m/z* 371.1634 $[M+H]^+$; calcd for $C_{20}H_{24}N_4OCl$, 371.1633. Yellow-brown solid, yield 73%.

*4.1.1.20. (E)-N′-((1-(2-chlorobenzyl)piperidin-4-yl)methylene)-N-methylpicolinohydrazide (**20**).* ^{1}H NMR (400 MHz, $CDCl_3$) δ 1.36–1.50 (2H, m), 1.65 (2H, d, J = 12.3 Hz), 2.07 (2H, t, J = 11.2 Hz), 2.11–2.23 (1H, m), 2.80 (2H, d, J = 10.6 Hz), 3.39 (3H, s), 3.56 (2H, s), 7.03 (1H, d, J = 3.4 Hz), 7.13–7.25 (2H, m), 7.25–7.36 (2H, m), 7.42 (2H, d, J = 7.2 Hz), 7.72 (1H, t, J = 7.7 Hz), 8.62 (1H, d, J = 3.9 Hz). ^{13}C NMR (101 MHz, $CDCl_3$) δ 28.01, 29.26, 38.78, 53.00, 59.43, 122.95, 123.68, 126.55, 128.01, 129.35, 130.60, 134.21, 135.75, 136.13, 146.29, 148.73, 154.86, 169.69. HRMS (ESI): *m/z* 371.1635 $[M+H]^+$; calcd for $C_{20}H_{24}N_4OCl$, 371.1633. Yellowish brown oily liquid, yield 80%.

*4.1.1.21. (E)-N′-(1-(1-(2-chlorobenzyl)piperidin-4-yl)propylidene) picolinohydrazide (**21**).* ^{1}H NMR (400 MHz, $CDCl_3$) δ 1.20 (3H, t, J = 7.7 Hz), 1.71–1.88 (4H, m), 2.07–2.20 (2H, m), 2.42 (2H, q, J = 7.7 Hz), 2.48–2.60 (1H, m), 2.99 (2H, d, J = 11.3 Hz), 3.61 (2H, s), 7.13–7.19 (1H, m), 7.19–7.25 (1H, m), 7.29–7.35 (1H, m), 7.41–7.47 (1H, m), 7.50 (1H, d, J = 7.1 Hz), 7.86 (1H, dt, J = 1.5, 7.7 Hz), 8.28 (1H, d, J = 7.8 Hz), 8.54 (1H, d, J = 4.3 Hz), 10.87 (1H, s). ^{13}C NMR (101 MHz, $CDCl_3$) δ 10.14, 20.34, 29.49, 44.93, 53.59, 59.50, 122.81, 126.49, 126.56, 127.93, 129.35, 130.51, 134.17, 136.38, 137.55, 148.11, 149.72, 159.78, 165.21. HRMS (ESI): *m/z* 385.1797 $[M+H]^+$; calcd for $C_{21}H_{26}N_4OCl$, 385.1790. Light yellow oily liquid, yield 70%.

*4.1.1.22. (E)-N′-(1-(1-(2-chlorobenzyl)piperidin-4-yl)butylidene) picolinohydrazide (**22**).* ^{1}H NMR (400 MHz, $CDCl_3$) δ 1.09 (3H, t, J = 7.3 Hz), 1.60–1.69 (2H, m), 1.74–1.84 (4H, m), 2.09–2.19 (2H, m), 2.33–2.43 (2H, m), 2.45–2.56 (1H, m), 2.99 (2H, d, J = 11.4 Hz), 3.61 (2H, s), 7.14–7.26 (2H,m), 7.34 (1H, d, J = 8.0 Hz), 7.46 (1H, dd, J = 4.9, 6.7 Hz), 7.51 (1H, d, J = 7.4 Hz), 7.88 (1H, dt, J = 1.5, 7.7 Hz), 8.30 (1H, d, J = 7.8 Hz), 8.56 (1H, d, J = 4.5 Hz), 10.89 (1H, s). ^{13}C NMR (101 MHz, $CDCl_3$) δ 14.71, 19.35, 29.57, 29.61, 44.94, 53.64, 59.48, 122.77, 126.47, 126.57, 127.93, 129.33, 130.52, 134.14, 136.36, 137.55, 148.13, 149.74, 159.67, 164.34. HRMS (ESI): *m/z* 399.1947 $[M+H]^+$; calcd for $C_{22}H_{28}N_4OCl$, 399.1946. Brown solid, yield 76%.

*4.1.1.23. (E)-N′-(1-(1-(2-chlorobenzyl)piperidin-4-yl)pentylidene) picolinohydrazide (**23**).* ^{1}H NMR (400 MHz, $CDCl_3$) δ 1.00 (3H, t, J = 7.1 Hz), 1.43–1.63 (4H, m), 1.71–1.88 (4H, m), 2.07–2.22 (2H, m), 2.33–2.43 (2H, m), 2.46–2.58 (1H, m), 2.99 (2H, d, J = 11.0 Hz), 3.62 (2H, s), 7.13–7.20 (1H, m), 7.23 (1H, t, J = 7.1 Hz), 7.33 (1H, d, J = 7.8 Hz), 7.41–7.47 (1H, m), 7.51 (1H, d, J = 7.1 Hz), 7.86 (1H, dt, J = 1.4, 7.7 Hz), 8.28 (1H, d, J = 7.8 Hz), 8.54 (1H, d, J = 4.4 Hz), 10.90 (1H, s). ^{13}C NMR (101 MHz, $CDCl_3$) δ 13.68, 23.22, 27.21, 27.72, 29.54, 44.95, 53.59, 59.43, 122.74, 126.48, 126.60, 128.00, 129.34, 130.60, 134.17, 137.55, 148.07, 149.73, 159.66, 164.42. HRMS (ESI): *m/z* 413.2105 $[M+H]^+$; calcd for $C_{23}H_{30}N_4OCl$, 413.2103. Brown solid, yield 74%.

*4.1.1.24. (E)-N′-(1-(1-(2-chlorobenzyl)piperidin-4-yl)-3-methylbutylidene)picolinohydrazide (**24**).* ^{1}H NMR (400 MHz, $CDCl_3$) δ 1.05 (6H, d, J = 6.6 Hz), 1.74–1.94 (4H, m), 2.07–2.23 (3H, m), 2.30 (2H, d, J = 7.5 Hz), 2.36–2.48 (1H, m), 3.00 (2H, d, J = 10.1 Hz), 3.62 (2H, s), 7.17 (1H, t, J = 7.0 Hz), 7.24 (1H, t, J = 7.2 Hz), 7.33 (1H, d, J = 7.8 Hz), 7.45 (1H, dd, J = 4.9, 6.7 Hz), 7.53 (1H, d, J = 7.3 Hz), 7.87 (1H, dt, J = 1.5, 7.7 Hz), 8.29 (1H, d, J = 7.8 Hz), 8.56 (1H, d, J = 4.5 Hz), 10.93 (1H, s). ^{13}C NMR (101 MHz, $CDCl_3$) δ 23.19, 26.71, 30.00, 37.02, 44.84, 53.79, 59.34, 122.75, 126.42, 126.62, 127.92, 129.28, 130.54, 134.07, 136.33, 137.54, 148.11, 149.81, 159.55, 163.73. HRMS (ESI): *m/z* 413.2105 $[M+H]^+$; calcd for $C_{23}H_{30}N_4OCl$, 413.2103. Light yellow solid, yield 51%.

4.2. Biology

4.2.1. In vitro AChE and BChE inhibition Assays.

The enzyme inhibition activity of the test compounds was performed adopting the method of Ellman et al.[35]. Electric eel acetyl cholinesterase (eeAChE) and horse serum butyryl cholinesterase (eqBChE) were purchased from Sigma. 5,5′-dithiobis(2-nitrobenzoic acid) (DTNB-Ellman's reagent), acetylthiocholine iodide (ATCI), butyrylthiocholine iodide (BTCI), tacrine and donepezil were purchased from Aladdin (Shanghai, China). All the experiments were conducted in Corning Costar 96-well clear flat-bottom plates (9017). The experiment medium was 50 mM sodium phosphate buffer at pH 8 with a final concentration of 0.5% DMSO and 0.01% Triton-X100.

Briefly, 50 μL of AChE or 50 μL of BChE and 100 μL of the compound were incubated in 96-well plates at room temperature for 10 min. Further, a mixture of 25 μL of the substrate, ATCI (5 mM) or BTCI (5 mM), and 25 μL of DTNB (5 mM) were added to each well to start the reaction. After 30 min of reaction time in the dark, the absorbance was measured at 415 nm wavelength using microplate reader FlexStation 3 (Molecular Devices, US).

The IC_{50} value was calculated from the absorbance obtained for various concentrations of the test and the standard compounds. All the determinations were performed in triplicate and at least in three independent runs. The enzyme kinetic study was done to determine the mechanism of AChE inhibition by donepezil and compound **21** in a similar manner as described above.

4.2.2. Metal Chelation [49]

Compound 21 was tested as a metal chelating agent using a differential UV–visible spectrum with a wavelength range of 190–600 nm

recorded in phosphate buffer containing 0.05% DMSO in volume in room temperature. Compound 21 and several metal salts were formulated into 200 μM solutions. The metal salt solution was mixed with an equal volume of phosphate buffer as the background. A mixture of the compound 21 solution and an equal volume of phosphate buffer was used as the control group. The compound 21 solution was mixed with an equal volume of the metal salt solution and was allowed to stand for 30 min before measuring. The individual metal and solvent spectra were subtracted from the background to obtain the UV–vis spectrums that produced a change in absorption peak due to the complexation of the metal with compound 21.

4.2.3. Cytotoxicity Assay

Compound **10**, compound **21** and donepezil were tested for their cytotoxicity in rat phaeochromocytoma cell line PC12 using the vital mitochondrial function MTT assay with the Promega CellTiter 96® AQueous One Solution Reagent (contains MTS (3-(4,5-dimethylthiazol-2-yl)-5-(3-carboxymethoxyphenyl)-2-(4-sulfophenyl)-2H-tetrazolium) and PES (phenazine ethosulfate)). Poorly differentiated PC12 cells were supplied by the Cell Bank of the Kunming Institute of Zoology, CAS (Kunming, China). Cells were cultured in Dulbecco's Modified Eagle's Medium (DMEM, High Glucose) supplemented with 10% FBS, 100 units/mL penicillin and 100 μg/mL streptomycin at 37 °C in 5% CO_2 atmosphere. Poorly differentiated PC12 cells (10000 cell/well) were seeded in 96-well plates and incubated for 24 h. The culture medium was replaced with fresh medium (with 20 μM of compound **10**, compound **21** or donepezil) and the plates were returned to the incubator for 24 h. After drug treatments, the cells were cultured with fresh medium (CellTiter 96® AQueous One Solution Reagent/supplemented DMEM = 1:4 in volume) at 37 °C for 2 h. The absorbance was measured at 492 nm with a microplate reader. Cell viability was expressed as a percentage relative to the blank group. Data are expressed as means ± SD (n = 3).

4.2.4. Parallel artificial membrane permeability assay (PAMPA)

The Corning Gentest™ Pre-coated PAMPA Plate System was purchased from Innochem. The solutions of compounds **1**, **7**, **10**, **19**, **21**, **22** and donepezil in PBS buffer (pH = 7.4) were prepared from 10 mM stocks in DMSO respectively. The final DMSO concentration was adjusted to 3% in volume. The compounds and donepezil solution was added 300 μL/well to the donor wells at 200 μM concentration. The filter acceptor plate with 200 μL/well of PBS (with 3% DMSO) was carefully placed over the donor plate. All compounds were examined in quintuplicate. After 5 h incubation at room temperature, the plates were separated. The 100 μL of solution was transferred from acceptor and donor wells respectively to the Corning UV-Transparent 96-well plate (catalog #3635). The absorbance was measured at specific wavelengths determined for each compound using microplate reader FlexStation 3 (Molecular Devices, US). Calibration curves were generated for all compounds and donepezil at specific wavelengths respectively with correlation coefficients (R^2) over 0.99. The permeability coefficients (Pe, cm/s) and mass retention (R, %) of the compounds and donepezil were calculated according to the following formula introduced in the Gentest™ protocol.

4.3. Molecular modelling

The crystal structure of AChE complexed with donepezil (PDB code: 4EY7) and BChE complexed with HUN613 (PDB code: 6QAA) were extracted from the Protein Data Bank (https://www.rcsb.org/) with a resolution of 2.35 and 1.90 Å, respectively. The Prepare Protein module in Discovery Studio 4.0 (DS 4.0,Accelrys Inc., San Diego, CA, USA.) was used to prepare the structures. Sybyl-X 2.0 (Tripos, Inc., USA) was used to prepare the compounds. The Powell gradient algorithm was used to minimize structural energy. The position of donepezil and HUN613 were defined as the active center for docking, and the coordinate of the center points (x, y, z) were (-13.985, −43.975, 27.895) and (19.143, 42.419, 41.008), respectively. The Genetic Optimization of Ligand Docking (GOLD 5.2.2, CCDC) was used for docking studies. Both radius of two sphere were set to 10 Å, the template and the scoring function to the AChE and BChE were set chemscore_kinase and CHEMPLP. Tyr-341, Tyr-124, Phe-338, Phe-295 were set to be flexible to better predict possible interaction sites for the alkyl side chain of the compound. The rotatable torsion in the side chain and other parameters were set as default parameters. The genetic algorithms (GA) Runs was set to 50 times.

Declaration of Competing Interest

The authors declared that they have no conflicts of interest to this work.

We declare that we do not have any commercial or associative interest that represents a conflict of interest in connection with the work submitted.

Acknowledgements

This project was financially supported by the Grant of Sichuan Science and Technology Program (No: 19ZDYF1034), General Program of Applied Basic Research of Yunnan Province (No: 2014FB174), and the State Key Laboratory of Phytochemistry and Plant Resources in West China (No. P2017-KF07, P2018-KF14).

Appendix A. Supplementary material

Supplementary data to this article can be found online at https://doi.org/10.1016/j.bioorg.2019.103322.

References

[1] A.S. Association, Alzheimer's disease facts and figures, Alzheimer's Dementia 13 (4) (2017) 325–373.
[2] World Health Organization, “10 facts on dementia”, April 2017, https://www.who.int/features/factfiles/dementia/en/, (accessed September 9th, 2019).
[3] E.J. Mufson, M.D. Ikonomovic, S.E. Counts, S.E. Perez, M. Malek-Ahmadi, S.W. Scheff, S.D. Ginsberg, Molecular and cellular pathophysiology of preclinical Alzheimer's disease, Behav. Brain Res. 311 (2016) 54–69 https://www.ncbi.nlm.nih.gov/pubmed/27185734.
[4] R. Schliebs, T. Arendt, The significance of the cholinergic system in the brain during aging and in Alzheimer's disease, J Neural Transm (Vienna) 113 (11) (2006) 1625–1644 https://www.ncbi.nlm.nih.gov/pubmed/17039298.
[5] B.A.I, T.R.E, Therapeutics for Alzheimer’s disease based on the metal hypothesis, Neurotherapeutics the Journal of the American Society for Experimental Neurotherapeutics 5 (3) (2008) 421–432.
[6] M.G. Savelieff, G. Nam, J. Kang, H.J. Lee, M. Lee, M.H. Lim, Development of multifunctional molecules as potential therapeutic candidates for alzheimer's disease parkinson's disease, and amyotrophic lateral sclerosis in the last decade, Chem. Rev. 119 (2) (2019) 1221–1322 https://www.ncbi.nlm.nih.gov/pubmed/30095897.
[7] D. Strozyk, L.J. Launer, P.A. Adlard, R.A. Cherny, A. Tsatsanis, I. Volitakis, K. Blennow, H. Petrovitch, L.R. White, A.I. Bush, Zinc and copper modulate Alzheimer Abeta levels in human cerebrospinal fluid, Neurobiol. Aging 30 (7) (2009) 1069–1077 https://www.ncbi.nlm.nih.gov/pubmed/18068270.
[8] K.P. Kepp, Bioinorganic chemistry of Alzheimer's disease, Chem. Rev. 112 (10) (2012) 5193–5239 https://www.ncbi.nlm.nih.gov/pubmed/22793492.
[9] M.A. Greenough, J. Camakaris, A.I. Bush, Metal dyshomeostasis and oxidative stress in Alzheimer's disease, Neurochem. Int. 62 (5) (2013) 540–555 https://www.ncbi.nlm.nih.gov/pubmed/22982299.
[10] S. Bagheri, R. Squitti, T. Haertle, M. Siotto, A.A. Saboury, Role of copper in the onset of alzheimer's disease compared to other metals, Front Aging Neurosci 9 (2017) 446 https://www.ncbi.nlm.nih.gov/pubmed/29472855.
[11] S.K.A. Opare, A. Rauk, Copper(I) Chelators for Alzheimer's Disease, J. Phys. Chem. B 121 (50) (2017) 11304–11310 https://www.ncbi.nlm.nih.gov/pubmed/29172520.
[12] M.R.D.C, T.R, F.C.A.M, Acylhydrazone derivatives: a patent review, Expert Opinion on Therapeutic Patents 24 (11) (2014) pp. 1161–1170.
[13] S. Thota, D.A. Rodrigues, P.S.M. Pinheiro, L.M. Lima, C.A.M. Fraga, E.J. Barreiro, N-Acylhydrazones as drugs, Bioorg. Med. Chem. Lett. 28 (17) (2018) 2797–2806 https://www.ncbi.nlm.nih.gov/pubmed/30006065.
[14] D.R. Guay, An Update on the Role of Nitrofurans in the Management of Urinary Tract Infections, Drugs 61 (3) (2001) 353–364, https://doi.org/10.2165/

00003495-200161030-00004.
[15] M.C. Misra, Imlitemsu, drug treatment of haemorrhoids, Drugs 65 (11) (2005) 1481–1491, https://doi.org/10.2165/00003495-200565110-00003.
[16] B. Begovic, S. Ahmedtagic, L. Calkic, M. Vehabovic, S.B. Kovacevic, T. Catic, M. Mehic, Open clinical trial on using nifuroxazide compared to probiotics in treating acute diarrhoeas in adults, Mater. Sociomed. 28 (6) (2016) 454–458 https://www.ncbi.nlm.nih.gov/pubmed/28144199.
[17] J.C. Ruela Correa, Physico-chemical characterization and analytical development for sodium azumolene, a potential drug designed to fight malignant hyperthermia, J. Anal. Bioanalytical Tech. 05 (01) (2014).
[18] X. Ma, D.R. Gang, The *Lycopodium* alkaloids, Nat. Prod. Rep. 21 (6) (2004) 752–772 https://www.ncbi.nlm.nih.gov/pubmed/15565253.
[19] J.Y. Jia, Q.H. Zhao, Y. Liu, Y.Z. Gui, G.Y. Liu, D.Y. Zhu, C. Yu, Z. Hong, Phase I study on the pharmacokinetics and tolerance of ZT-1, a prodrug of huperzine A, for the treatment of Alzheimer's disease, Acta. Pharmaceutica Sinica 34 (7) (2013) 976–982 https://www.ncbi.nlm.nih.gov/pubmed/23624756.
[20] X. Ma, C. Tan, D. Zhu, D.R. Gang, P. Xiao, Huperzine A from Huperzia species–an ethnopharmacolgical review, J. Ethnopharmacol. 113 (1) (2007) 15–34 https://www.ncbi.nlm.nih.gov/pubmed/17644292.
[21] P.B. Watkins, H.J. Zimmerman, M.J. Knapp, S.I. Gracon, K.W. Lewis, Hepatotoxic effects of tacrine administration in patients with Alzheimer's disease, J. Am. Med. Assoc. 271 (13) (1994) 992–998, https://doi.org/10.1001/jama.1994.03510370044030.
[22] A.R. Punga, M. Sawada, E.V. Stålberg, Electrophysiological signs and the prevalence of adverse effects of acetylcholinesterase inhibitors in patients with myasthenia gravis, Muscle. Nerve. 37 (3) (2008) 300–307 https://onlinelibrary.wiley.com/doi/abs/10.1002/mus.20935.
[23] J. Cheung, M.J. Rudolph, F. Burshteyn, M.S. Cassidy, E.N. Gary, J. Love, M.C. Franklin, J.J. Height, Structures of human acetylcholinesterase in complex with pharmacologically important ligands, J. Med. Chem. 55 (22) (2012) 10282–10286 https://www.ncbi.nlm.nih.gov/pubmed/23035744.
[24] A. Meden, D. Knez, M. Jukic, X. Brazzolotto, M. Grsic, A. Pislar, A. Zahirovic, J. Kos, F. Nachon, J. Svete, S. Gobec, U. Groselj, Tryptophan-derived butyrylcholinesterase inhibitors as promising leads against Alzheimer's disease, Chem. Commun. (Camb.) 55 (26) (2019) 3765–3768 https://www.ncbi.nlm.nih.gov/pubmed/30864579.
[25] A. Shafferman, C. Kronman, Y. Flashner, M. Leitner, H. Grosfeld, A. Ordentlich, Y. Gozes, S. Cohen, N. Ariel, et al., Mutagenesis of human acetylcholinesterase. Identification of residues involved in catalytic activity and in polypeptide folding, J. Biol. Chem. 267 (25) (1992) 17640–17648 http://www.jbc.org/content/267/25/17640.abstract.
[26] M. Unzeta, G. Esteban, I. Bolea, W.A. Fogel, R.R. Ramsay, M.B. Youdim, K.F. Tipton, J. Marco-Contelles, Multi-target directed donepezil-like ligands for Alzheimer's disease, Front. Neurosci. 10 (2016) 205 https://www.ncbi.nlm.nih.gov/pubmed/27252617.
[27] Z. Temesgen, J. Feinberg, Tipranavir: a new option for the treatment of drug-resistant HIV infection, Clin. Infect. Dis. 45 (6) (2007) 761–769 https://www.ncbi.nlm.nih.gov/pubmed/17712762.
[28] B. Escudier, T. Eisen, W.M. Stadler, C. Szczylik, S. Oudard, M. Siebels, S. Negrier, C. Chevreau, E. Solska, A.A. Desai, F. Rolland, T. Demkow, T.E. Hutson, M. Gore, S. Freeman, B. Schwartz, M. Shan, R. Simantov, R.M. Bukowski, Sorafenib in advanced clear-cell renal-cell carcinoma, N. Engl. J. Med. 356 (2) (2007) 125–134, https://doi.org/10.1056/NEJMoa060655.
[29] Z. Sang, K. Wang, P. Zhang, J. Shi, W. Liu, Z. Tan, Design, synthesis, in-silico and biological evaluation of novel chalcone derivatives as multi-function agents for the treatment of Alzheimer's disease, Eur. J. Med. Chem. 180 (2019) 238–252 http://www.sciencedirect.com/science/article/pii/S0223523419306427.
[30] G. Gutti, D. Kumar, P. Paliwal, A. Ganeshpurkar, K. Lahre, A. Kumar, S. Krishnamurthy, S.K. Singh, Development of pyrazole and spiropyrazoline analogs as multifunctional agents for treatment of Alzheimer's disease, Bioorg. Chem. 90 (2019) 103080 http://www.sciencedirect.com/science/article/pii/S0045206819305930.
[31] K. Czarnecka, M. Girek, K. Maciejewska, R. Skibiński, J. Jończyk, M. Bajda, J. Kabziński, P. Sołowiej, I. Majsterek, P. Szymański, New cyclopentaquinoline hybrids with multifunctional capacities for the treatment of Alzheimer's disease, J. Enzyme Inhib. Med. Chem. 33 (1) (2018) 158–170, https://doi.org/10.1080/14756366.2017.1406485.
[32] Y. Wang, Y. Sun, Y. Guo, Z. Wang, L. Huang, X. Li, Dual functional cholinesterase and MAO inhibitors for the treatment of Alzheimer's disease: synthesis, pharmacological analysis and molecular modeling of homoisoflavonoid derivatives, J. Enzyme Inhib. Med. Chem. 31 (3) (2016) 389–397, https://doi.org/10.3109/14756366.2015.1024675.
[33] J. Yan, J. Hu, A. Liu, L. He, X. Li, H. Wei, Design, synthesis, and evaluation of multitarget-directed ligands against Alzheimer's disease based on the fusion of donepezil and curcumin, Bioorg. Med. Chem. Lett. 25 (12) (2017) 2946–2955 https://www.ncbi.nlm.nih.gov/pubmed/28454848.
[34] L. M. Lima, G. Zapata-Sudo, I. K. da Costa Nunes, J. Segundo Chaves de Araujo, J. da Silva, M. Manhães Trachez, T. Fernandes da Silva, F. P. da Costa, R. Sudo, E. Barreiro, Synthesis, solubility, plasma stability, and pharmacological evaluation of novel sulfonylhydrazones designed as anti-diabetic agents, Drug Design, Development and Therapy 10 (2016) pp. 2869–2879.
[35] G.L. Ellman, K.D. Courtney, V. Andres, R.M. Featherstone, A new and rapid colorimetric determination of acetylcholinesterase activity, Biochem. Pharmacol. 7 (2) (1961) 88–95 http://www.sciencedirect.com/science/article/pii/0006295261901459.
[36] O. Di Pietro, F.J. Pérez-Areales, J. Juárez-Jiménez, A. Espargaró, M.V. Clos, B. Pérez, R. Lavilla, R. Sabaté, F.J. Luque, D. Muñoz-Torrero, Tetrahydrobenzo[h][1,6]naphthyridine-6-chlorotacrine hybrids as a new family of anti-Alzheimer agents targeting β-amyloid, tau, and cholinesterase pathologies, Eur. J. Med. Chem. 84 (2014) 107–117 http://www.sciencedirect.com/science/article/pii/S0223523414006278.
[37] S. Gupta, A. Fallarero, P. Järvinen, D. Karlsson, M.S. Johnson, P.M. Vuorela, C.G. Mohan, Discovery of dual binding site acetylcholinesterase inhibitors identified by pharmacophore modeling and sequential virtual screening techniques, Bioorg. Med. Chem. Lett. 21 (4) (2011) 1105–1112 http://www.sciencedirect.com/science/article/pii/S0960894X10018950.
[38] G. Kryger, I. Silman, J.L. Sussman, Three-dimensional structure of a complex of E2020 with acetylcholinesterase from *Torpedo californica*, J. Phys.-Paris 92 (3) (1998) 191–194 http://www.sciencedirect.com/science/article/pii/S0928425798800089.
[39] C. de Los Rios, J. Marco-Contelles, Tacrines for Alzheimer's disease therapy. III. The PyridoTacrines, Eur. J. Med. Chem. 166 (2019) 381–389 https://www.ncbi.nlm.nih.gov/pubmed/30739821.
[40] K.A. Petrov, A.D. Kharlamova, O.A. Lenina, A.R. Nurtdinov, M.E. Sitdykova, V.I. Ilyin, I.V. Zueva, E.E. Nikolsky, Specific inhibition of acetylcholinesterase as an approach to decrease muscarinic side effects during myasthenia gravis treatment, Sci. Rep. 8 (1) (2018) 304 https://www.ncbi.nlm.nih.gov/pubmed/29321572.
[41] R. Azzouz, L. Peauger, V. Gembus, M. L. Tintas, J. Sopkova-de Oliveira Santos, C. Papamicael, V. Levacher, Novel donepezil-like N-benzylpyridinium salt derivatives as AChE inhibitors and their corresponding dihydropyridine "bio-oxidizable" prodrugs: Synthesis, biological evaluation and structure-activity relationship, Eur J Med Chem 145 (2018) pp. 165–190. https://www.ncbi.nlm.nih.gov/pubmed/29324339.
[42] L. Li, H.Y. Sun, W. Liu, H.Y. Zhao, M.L. Shao, Silymarin protects against acrylamide-induced neurotoxicity *via* Nrf2 signalling in PC12 cells, Food Chem. Toxicol. 102 (2017) 93–101 https://www.ncbi.nlm.nih.gov/pubmed/28137608.
[43] G. Latacz, A. Lubelska, M. Jastrzębska-Więsek, A. Partyka, K. Kucwaj-Brysz, A. Wesołowska, K. Kieć-Kononowicz, J. Handzlik, MF-8, a novel promising arylpiperazine-hydantoin based 5-HT7 receptor antagonist: In vitro drug-likeness studies and in vivo pharmacological evaluation, Bioorg. Med. Chem. Lett. 28 (5) (2018) 878–883 http://www.sciencedirect.com/science/article/pii/S0960894X18300842.
[44] P. Hochegger, J. Faist, W. Seebacher, R. Saf, P. Mäser, M. Kaiser, R. Weis, Synthesis and structure-activity relationships for new 6-fluoroquinoline derivatives with antiplasmodial activity, Biorg. Med. Chem. 27 (10) (2019) 2052–2065 http://www.sciencedirect.com/science/article/pii/S0968089619302664.
[45] A.S. Hogendorf, A. Hogendorf, K. Popiołek-Barczyk, A. Ciechanowska, J. Mika, G. Satała, M. Walczak, G. Latacz, J. Handzlik, K. Kieć-Kononowicz, E. Ponimaskin, S. Schade, A. Zeug, M. Bijata, M. Kubicki, R. Kurczab, T. Lenda, J. Staroń, R. Bugno, B. Duszyńska, B. Pilarski, A.J. Bojarski, Fluorinated indole-imidazole conjugates: Selective orally bioavailable 5-HT7 receptor low-basicity agonists, potential neuropathic painkillers, Eur. J. Med. Chem. 170 (2019) 261–275 http://www.sciencedirect.com/science/article/pii/S0223523419302284.
[46] K. Socała, S. Mogilski, M. Pieróg, D. Nieoczym, M. Abram, B. Szulczyk, A. Lubelska, G. Latacz, U. Doboszewska, P. Wlaź, K. Kamiński, KA-11, a Novel Pyrrolidine-2,5-dione Derived Broad-Spectrum Anticonvulsant: Its Antiepileptogenic, Antinociceptive Properties and *in vitro* Characterization, ACS Chem. Neurosci. 10 (1) (2019) 636–648, https://doi.org/10.1021/acschemneuro.8b00476.
[47] Z. Liang, Q.X. Li, Discovery of Selective, Substrate-Competitive, and Passive Membrane Permeable Glycogen Synthase Kinase-3β Inhibitors: Synthesis, Biological Evaluation, and Molecular Modeling of New C-Glycosylflavones, ACS Chem. Neurosci. 9 (5) (2018) 1166–1183, https://doi.org/10.1021/acschemneuro.8b00010.
[48] X. Chen, A. Murawski, K. Patel, C.L. Crespi, P.V. Balimane, A Novel Design of Artificial Membrane for Improving the PAMPA Model, Pharm. Res. 25 (7) (2008) 1511–1520, https://doi.org/10.1007/s11095-007-9517-8.
[49] L. Huang, C. Lu, Y. Sun, F. Mao, Z. Luo, T. Su, H. Jiang, W. Shan, X. Li, Multitarget-directed benzylideneindanone derivatives: anti-beta-amyloid (Abeta) aggregation, antioxidant, metal chelation, and monoamine oxidase B (MAO-B) inhibition properties against Alzheimer's disease, J. Med. Chem. 55 (19) (2012) 8483–8492 https://www.ncbi.nlm.nih.gov/pubmed/22978824.